Neurobiology of Disease 214 (2025) 107029

Contents lists available at ScienceDirect

Neurobiology of Disease

journal homepage: www.elsevier.com/locate/ynbdi

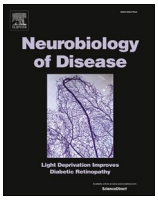

# Elevated 24-hydroxycholesterol levels counteract okadaic acid-induced tau hyperphosphorylation and neuronal morphology impairment

Serena Giannelli [a,b], Francesca Eroli [b], Raúl Loera-Valencia [b,c], Valerio Leoni [d], Maria Latorre-Leal [b], Gabriella Testa [a], Erica Staurenghi [a], Barbara Sottero [a], Paola Gamba [a], Silvia Maioli [b,*,1], Gabriella Leonarduzzi [a,*,1]

[a] Department of Clinical and Biological Sciences, University of Turin, San Luigi Hospital, Orbassano, Turin, Italy
[b] Department of Neurobiology Care Sciences and Society, Division of Neurogeriatrics, Center for Alzheimer Research, Karolinska Institutet, Stockholm, Sweden
[c] Tecnologico de Monterrey, School of Medicine and Health Sciences, Chihuahua, Mexico
[d] Laboratory of Clinical Pathology, Hospital Pio XI of Desio, ASST-Brianza and Department of Medicine and Surgery, University of Milano-Bicocca, Desio, Italy

ARTICLE INFO

*Keywords:*
24-hydroxycholesterol
CYP46A1
Tau hyperphosphorylation
Tau oligomers
Dendritic arborization
Alzheimer's disease

ABSTRACT

Multiple findings underline a link between altered brain cholesterol metabolism and Alzheimer's disease (AD) pathogenesis. Physiologically, excess brain cholesterol is mainly converted into 24-hydroxycholesterol (24-OHC) by the neuron-specific enzyme CYP46A1. Of note, we previously observed in autopsy specimens from human AD brains that 24-OHC and, in parallel, *CYP46A1* expression decrease at advanced stages, suggesting a possible cause-effect between these reductions and AD progression. In the present study, we aimed to investigate whether maintaining high levels of 24-OHC, by its exogenous administration or *CYP46A1* overexpression, can counteract tau hyperphosphorylation and accumulation of prefibrillar tau oligomers. To create an AD-like *in vitro* model exhibiting tauopathy, we utilized okadaic acid (OKA), a chemical compound that induces tau hyperphosphorylation. Our data show that in 24-OHC-treated primary neurons derived from wild type mice and in neurons from *CYP46A1* overexpressing mice (CYP46Tg) elevated oxysterol levels effectively prevented tau hyperphosphorylation and oligomerization. Furthermore, the dendritic arborization decrease induced by OKA was prevented, maintaining the organization and stability of the neuronal cytoskeleton. While hypothesized underlying molecular mechanisms (GSK3β, CDK5, ERK1/2, and PP2A) seem not to be involved, the protective effect of 24-OHC remains evident. The data highlight the positive effects of 24-OHC and the need to prevent its reduction in the brain. This can be achieved either through the exogenous administration of 24-OHC using suitable technologies or by maintaining elevated levels and the activity of the enzyme CYP46A1. These therapeutic approaches could be useful to prevent or slow AD progression.

## 1. Introduction

Neurofibrillary tangles (NFTs), a primary neuropathologic trademark promoting dysfunction and neurodegeneration in Alzheimer's disease (AD), are composed of aberrantly phosphorylated tau protein, which accumulates in the perinuclear cytoplasm of neurons in the form of paired-helical filaments (PHFs) (Ballatore et al., 2007; Grundke-Iqbal et al., 1986).

Tau is a microtubule-associated protein predominantly localized in neuronal axons where its primary function is to promote not only the

*Abbreviations:* 24-OHC, 24-hydroxycholesterol; AD, Alzheimer's disease; Aβ, amyloid β; BBB, blood-brain barrier; BCA, bicinchoninic acid; BSA, bovine serum albumin; CDK5, cyclin-dependent kinase 5; CE, cholesteryl esters; CYP46Tg, overexpressing human CYP46A1 HA-tagged transgenic mice; DAPI, 4′,6-diamidino-2-phenylindole; EDTA, ethylenediaminetetraacetic acid; EFV, Efavirenz; EGTA, ethyleneglycol-bis(β-aminoethyl)-N,N,N′,N′,-tetraacetic acid; ER, estrogen receptor; ERK1/2, extracellular signal-regulated kinase 1/2; GC–MS, gas chromatography mass spectrometry; GSK3β, glycogen synthase kinase 3β; iPSC, induced pluripotent stem cells; LDH, lactate dehydrogenase; MAP2, microtubule associated protein 2; MAPK, mitogen-activated protein kinase; NFT, neurofibrillary tangle; NMDAR, *N*-methyl-D-aspartate receptor; OKA, okadaic acid; PBS, phosphate-buffered saline; PHF, paired-helical filament; PP, protein phosphatase; SIRT1, sirtuin 1; TBS, Tris-buffered saline; UPS, ubiquitin-proteasome system; WT, wild type.

* Corresponding authors.
*E-mail addresses:* silvia.maioli@ki.se (S. Maioli), gabriella.leonarduzzi@unito.it (G. Leonarduzzi).
[1] These authors contributed equally to this work.

https://doi.org/10.1016/j.nbd.2025.107029
Received 27 February 2025; Received in revised form 18 June 2025; Accepted 10 July 2025
Available online 11 July 2025

microtubule assembly and the axonal transport (Cleveland et al., 1977) but also the neurite outgrowth (Caceres and Kosik, 1990). Physiologically, a fine balance between the activity of several kinases, such as glycogen synthase kinase 3β (GSK3β), cyclin-dependent kinase 5 (CDK5), mitogen-activated protein kinase (MAPK), and protein phosphatase (PP) 2A keeps tau-microtubule interactions tightly regulated. In pathological conditions, an imbalance in tau kinase and phosphatase activity results in tau hyperphosphorylation, leading to tau-tau interactions, insoluble aggregate formation, and microtubule destabilization (Johnson and Stoothoff, 2004).

Changes in tau localization are associated with disease stages; indeed, the redistribution of hyperphosphorylated tau to the somatodendritic compartment is recognized as a key pathological marker in the early stage of tauopathy development. Tau deposits determine the dysfunction of axonal transport, the reduction of dendritic spines, and the impairment of synaptic transmission (Brunello et al., 2020). Based on the published literature, many studies define the prefibrillar tau oligomers as the most toxic form of tau responsible for synaptic impairment and for cognitive decline in AD before the appearance of NFTs; moreover, oligomers have a pivotal role in the pathology propagation (Brunden et al., 2008; Fá et al., 2016; Tai et al., 2014). For this reason, the prevention of tau aggregation and propagation is the focus of attempts to identify new potential therapeutic targets to modulate the mechanisms involved in this event.

Increasing epidemiological and molecular evidence supports the idea that hypercholesterolemia and the disruption of brain cholesterol homeostasis play a key role in AD pathogenesis (Ahmed et al., 2024; Gamba et al., 2012; Loera-Valencia et al., 2019). Brain cholesterol homeostasis is maintained through its de *novo* biosynthesis and its disposal in cholesterol oxidation products, named oxysterols. When cholesterol levels exceed physiological limits, it is mainly converted into the more hydrophilic metabolite sterol 24-hydroxycholesterol (24-OHC) by the enzyme CYP46A1 (*i.e.*, 24-hydroxylase), highly expressed across different brain regions such as basal ganglia, cortex, and hippocampus; CYP46A1 is responsible for at least 40 % of brain cholesterol conversion (Björkhem et al., 2009; Lund et al., 2003). The oxysterol 24-OHC, as well as other oxysterols, is capable of passing through the blood-brain barrier (BBB) and fluxing from the brain into the systemic circulation; however, other oxysterols may accumulate in the brain and others present in the systemic circulation may cross the BBB and accumulate in the brain too, contributing to the AD onset and progression (Gamba et al., 2015). Although high levels of some oxysterols cause neuron dysfunction and degeneration, a neuroprotective role has long been attributed to 24-OHC (Gamba et al., 2021); 24-OHC seems to have beneficial effects playing a pivotal role in the maintenance of brain cholesterol metabolism: it suppresses cholesterol biosynthesis in astrocytes by inhibiting sterol regulatory element-binding protein (SREBP) activation (Han et al., 2020) and stimulates the expression of liver X receptor (LXR)-responsive genes, such as ATP binding cassette subfamily A member 1 (ABCA1), ATP binding cassette subfamily G member 1 (ABCG1), and apolipoprotein E (ApoE), thus favoring cholesterol transport from astrocytes to neurons (Abildayeva et al., 2006). Moreover, the emerging hypothesis is that 24-OHC could act in the brain by stimulating neuroprotective pathways, such as sirtuin 1 (SIRT1)-dependent pathways, as demonstrated in recent studies by our laboratory (Testa et al., 2023; Testa et al., 2018).

A systematic analysis of oxysterols in *post-mortem* specimens from the frontal and occipital cortices of human AD brains, classified according to the Braak staging system of neurofibrillary pathology, highlighted that the levels of 24-OHC and, in parallel, the expression of *CYP46A1* decrease significantly with the progression of the disease; their loss is due to the progressive neuron death, suggesting it as a factor in accelerating AD progression (Testa et al., 2016). Recently, Varma and colleagues conducted a metabolomic and transcriptomic study on brain autopsy samples from the Baltimore Longitudinal Study of Aging (BLSA) and the Religious Orders Study (ROS), confirming that 24-OHC levels and *CYP46A1* expression are lower in AD brains and the lower 24-OHC concentration is associated with greater severity of both neuritic plaques and neurofibrillary pathology (Varma et al., 2021).

Although evidence has been reported about the modulation of amyloid precursor protein (APP) processing by 24-OHC and CYP46A1 activity (Hudry et al., 2010; Mast et al., 2017b), the relationship with tau pathology is still largely unexplored and debated. In this connection, injection of an adeno-associated virus (AAV)-CYP46A1 vector into the hippocampus of THY-tau22 mice, a model of AD-like tau pathology, rescued impaired long-term depression (LTD), a type of synaptic transmission, and other dendritic spine defects but did not affect tau phosphorylation and related gliosis (Burlot et al., 2015). Conversely, genetic inhibition of *CYP46A1* promoted the phosphorylation of tau protein (Djelti et al., 2015).

Based on these findings, we aimed to investigate in primary neurons whether elevated 24-OHC levels, either obtained by inducing the expression of *CYP46A1* or by exogenous 24-OHC administration, could prevent tau hyperphosphorylation and oligomerization. To obtain an AD-like *in vitro* model characterized by tauopathy, primary cultures of neurons were treated with okadaic acid (OKA). OKA selectively inhibits the ability of serine/threonine PP2A to dephosphorylate tau, thus inducing the accumulation of hyperphosphorylated tau protein. We compared the data obtained in neurons isolated from wild type (WT) mice and incubated with 24-OHC with those obtained in neurons isolated from *CYP46A1* overexpressing mice (CYP46Tg). Both 24-OHC treatment and *CYP46A1* overexpression prevented tau hyperphosphorylation, mainly at Thr231 residue, and oligomerization, and the dendritic arborization affected by OKA treatment was significantly prevented, preserving the organization and stability of the neuronal cytoskeleton. Molecular mechanisms hypothesized to be involved in the beneficial effects of 24-OHC in reducing tau phosphorylation were also investigated.

Our results point out that both exogenous sterol administration and *CYP46A1* overexpression could be promising therapeutic approaches to avoid 24-OHC loss in the brain during the AD progression and prevent the neurotoxic accumulation of hyperphosphorylated tau and the consequent neuronal damage.

## 2. Materials and methods

### 2.1. Cell cultures and treatments

Cortex and hippocampus were isolated from C57BL/6 J WT and human *CYP46A1* HA-tagged transgenic (CYP46Tg) embryonic mice at day 16–17 (E16–17). The overexpression of the *CYP46A1* gene was confirmed by tail genotyping (Transnetyx Automated Genotyping Center, Cordova, Shelby, TN, USA).

Primary cultures of cortico-hippocampal neurons were seeded into 6-well or 12-well plates previously coated with poly-D-lysine (10 μg/mL) (Sigma-Aldrich, Merck-Millipore, Darmstadt, Germany) and maintained in Neurobasal serum-free medium (Thermo Fisher Scientific, Waltham, MA, USA), supplemented with 2 % B-27 (Gibco, Thermo Fisher Scientific), 2 mM GlutaMAX (Thermo Fisher Scientific), 100 units/mL penicillin and 100 μg/mL streptomycin (PEST, Thermo Fisher Scientific), and incubated at 37 °C in a humidified 5 % $CO_2$-containing atmosphere. All treatments were performed after 10 days of cell culture (DIV 10). To assess the cytotoxicity and tau phosphorylation induced by OKA (Sigma-Aldrich), some primary neurons isolated from WT mice were incubated for 6 h with OKA at different concentrations (Supplementary Fig. 1A,B). In some experiments, primary neurons from WT mice were incubated with 1 μM 24-OHC (INstruchemie, Delfzijl, Netherlands) dissolved in ethanol (6.85 mM) for 10 h and then with or without OKA (dissolved in ethanol) at a non-cytotoxic concentration of 10 nM for 6 h or only with 1 μM 24-OHC (16 h). In others, primary neurons isolated from WT or CYP46Tg mice were incubated only with 10 nM OKA for 6 h. Vehicle (ethanol) was used as control. The experimental design is illustrated in

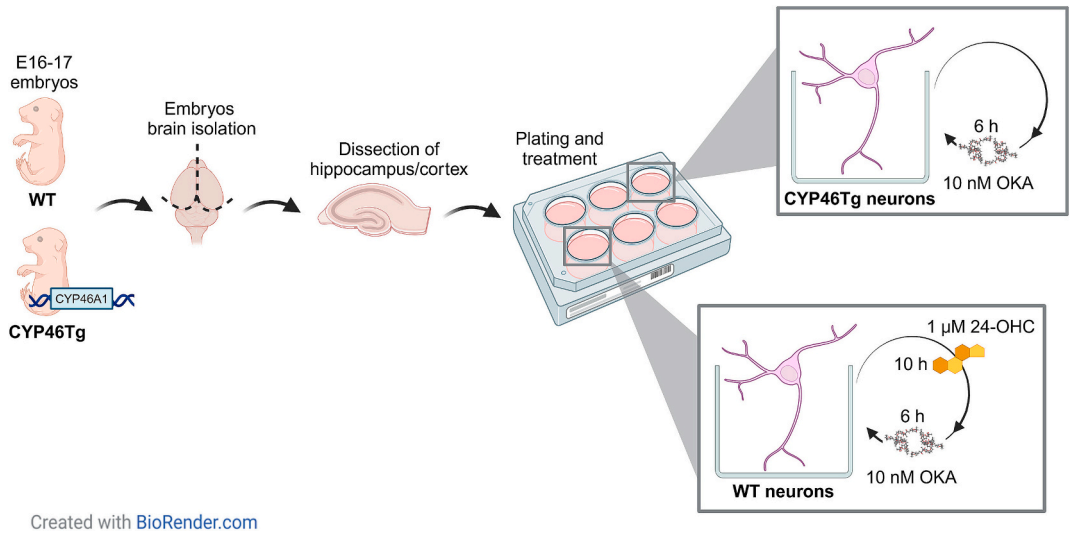


**Fig. 1.** Illustration of the experimental design of the work (created with BioRender.com). For a detailed explanation, see the "Materials and Methods" section.

Fig. 1. For all experiments, incubation times and concentrations are reported in the Results section and/or Figure legends.

### 2.2. Cytotoxicity assay

Lactate dehydrogenase (LDH) activity was quantified in the culture medium by employing a commercial kit (ab102526, Abcam, Cambridge, UK). Briefly, after centrifugation at maximum speed for 1 min at 4 °C to remove cell debris, media were diluted (1:5), and 50 μL of standard, positive control, or sample were loaded into a flat-bottom 96-well plate. Then, 50 μL of the reaction mix, containing LDH assay buffer and LDH substrate, were added to each well. After mixing, the LDH activity was measured at OD450 using a CLARIOstar plate reader (BMG LABTECH, Ortenberg, Germany); a kinetic mode was used: the samples were measured at 2 min intervals for 90 min at 37 °C. The LDH activity was calculated following the manufacturer's instructions and normalized against the amounts of proteins quantified in the respective cell lysates by Pierce bicinchoninic acid (BCA) Protein Assay Kit (Thermo Fisher Scientific).

### 2.3. 24-OHC quantification by GC–MS

The amount of 24-S-OHC was measured by isotope dilution gas chromatography–mass spectrometry (GC–MS). Cellular homogenates, prepared from pellets suspended in water (250 μL) and sonicated for 15 min, were transferred to a screw-capped vial sealed with a Teflon septum together with 50 ng of 24-R/S-OHC-25, 26, 26, 26, 27, 27, 27-d7 (Avanti Polar Lipids Inc., Birmingham, AL, USA) as internal standard, as well as 50 μL of butylated hydroxytoluene (BHT) (5 g/L) (Sigma-Aldrich) and 50 μL of K3-ethylenediaminetetraacetic acid (EDTA) (10 g/L) (Sigma-Aldrich) to prevent autoxidation. Each vial was flushed with argon for 10 min to remove air. Alkaline hydrolysis was carried out at room temperature for 1 h in the presence of ethanolic KOH 1 M. The oxysterol was extracted twice with 5 mL of cyclohexane, followed by centrifugation (3500 *g* for 10 min at 4 °C). The organic phase was evaporated under a gentle stream of argon and oxysterols converted into trimethylsilyl (TMS) ethers with 100 μL *N,O*-bis(trimethylsilyl)trifluoroacetamide (BSTFA) (Sigma-Aldrich) for 60 min at 70 °C. Isotope dilution GC–MS analysis was performed by a 6890 N Network GC system (Agilent Technologies, Santa Clara, CA, USA) equipped with an HP 7687 series autosampler and a HP 7683 series injector (Agilent Technologies) and coupled to a quadrupole mass selective detector HP5975B Inert MSD (Agilent Technologies). For GC separation a B-XLB column (30 m × 0.25 mm, i.d. 0.25 μm film thickness; J&W Scientific Alltech, Folsom, CA, USA) was used and the oven temperature program was as follows: an initial temperature of 180 °C held for 1 min, followed by a linear ramp of 20 °C/min to 270 °C, and then a linear ramp of 5 °C/min until the final temperature of 290 °C held for 11 min. Helium was used as a carrier gas at a flow rate of 1 mL/min. Injection of the sample (1 μL) was carried out in splitless mode, at 250 °C with a flow rate of 20 mL/min. The MS temperature parameters were 290 °C for the transfer line, 150 °C for the filament, and 220 °C for the quadrupole, according to the manufacturer's instructions. Mass spectrometric data were acquired in selected ion monitoring mode (TMS ethers) at $m/z = 420$ for 24-R/S-OHC-d7, $m/z = 413$ for 24-S-OHC.

Peak integration was performed manually, and the analyte was quantified from SIM analysis against internal standards using a standard curve. For each sample, the sterol amount was normalized to the corresponding number of cells present in the pellets (about $2 \times 10^6$).

### 2.4. Protein extraction and Western blotting

After treatments, cells were washed with phosphate-buffered saline (PBS) and lysed in ice-cold RIPA buffer (Thermo Fisher Scientific) supplemented with EDTA-Free Protease Inhibitor Cocktail (Roche, Basilea, Swiss) and phosphatase inhibitor cocktail 3 (Sigma-Aldrich) for 30 min, and then centrifuged at 13,800 *g* for 10 min at 4 °C. Total protein content was spectrophotometrically determined using the Pierce BCA Protein Assay Kit (Thermo Fisher Scientific).

To analyze the protein levels, 10 or 20 μg of total proteins were separated by electrophoresis in 10 % acrylamide gels and then transferred to nitrocellulose membranes (Amersham Protran, GE Healthcare, Chicago, IL, USA). After saturation of non-specific binding sites with 5 % non-fat dry milk in Tris-buffered saline (TBS) 1×-Tween 20 0.1 % for 1 h at room temperature, the membranes were immunoblotted overnight at 4 °C with the following primary antibodies: anti-AT180 (1:700, NB100–82249, Novus Biologicals, Englewood, CO, USA), anti-AT8 (1:500, MN1020, Invitrogen, Thermo Fisher Scientific), anti-tau (1:4000, A0024, Dako, Agilent Technologies, Santa Clara, CA, USA), anti-phosphoSer9-GSK3β (1:500, MA514873, Invitrogen), anti-phosphoTyr216-GSK3β (1:500, 44-604C, Invitrogen), anti-GSK3β (1:500, MA5–15597, Invitrogen), anti-p35 (1:500, sc-820, Santa Cruz Biotechnology, Dallas, TX, USA), anti-CDK5 (1:500, sc-173, Santa Cruz Biotechnology), anti-phospho-extracellular signal-regulated kinase 1/2 (ERK1/2) MAPK (Thr202/Tyr204) (1:500, 9101, Cell Signaling Technology, Danvers, MA, USA), anti-ERK1/2 MAPK (1:500, 4695, Cell Signaling Technology); or anti-actin (1:5000, A2066, Sigma-Aldrich) and anti-GAPDH (1:5000, AM4300, Invitrogen). After washing with

TBS-Tween 20 0.1 % to remove unbound primary antibodies, the membranes were probed with fluorophore-coupled (1:15000, LI-COR Biosciences, Lincoln, NE, USA) secondary anti-mouse or anti-rabbit antibodies for 1 h, at room temperature. Immunoreactivity was acquired by infrared fluorescence with the LI-COR Odyssey system (LI-COR Biosciences). The bands were quantified by densitometric analysis using the Image J 1.43 software.

### 2.5. Immunocytochemistry

Cortico-hippocampal neurons were plated on coverslips (18 mm diameter), previously coated with poly-D-lysine, into 12-well plates. After treatments, cells were washed with 0.01 M PBS, fixed in paraformaldehyde solution 4 % for 15 min at room temperature, and then washed again twice with PBS. After permeabilization and saturation of non-specific binding sites with 0.01 M PBS solution containing 1 % bovine serum albumin (BSA) and 0.1 % Triton X-100 for 1 h at room temperature, coverslips were incubated with the anti-T22 (1:500, Sigma-Aldrich) or anti-microtubule associated protein 2 (MAP2) (1:500, Abcam) primary antibodies, overnight at 4 °C; then, they were incubated, respectively, with the secondary antibody conjugated with fluorescent probes Alexa Fluor 546 (1:500, Invitrogen) or Alexa Fluor 488 (1:1000, Invitrogen) for 1 h, at room temperature. Nuclei were stained with 4′,6-diamidino-2-phenylindole (DAPI) (1 μg/mL, Thermo Fisher Scientific). After mounting with SlowFade Gold Antifade Mountant (Invitrogen), slides were observed using an LSM900-Airy confocal microscope (Carl Zeiss S.p.A., Oberkochen, Germany). At least one image for each condition was acquired from each biological replicate. The images were processed using Fiji ImageJ 1.53 t software. Moreover, the intensity of T22 fluorescence was analyzed in the soma of each neuron by applying the *Z*-project method (Projection type: sum slices) and expressed as integrated density (Mean Gray Value X Area).

### 2.6. Cell reconstruction

Neurons' images were reconstructed in 3D using the filament tracer tool of the Imaris software (BitPlane, South Windsor, CT, USA). The morphological parameters were determined by tracing the dendrites of the acquired neurons in a Z-stack file with no compression. No pixels were saturated in the acquired images. To assess the complexity of the dendritic arbors, the total number of intersections and total dendritic lengths were analyzed as a function of the distance from the soma, creating concentric spheres centered on the cell body of increasing 10-μm radii (Sholl analysis), as previously described (Merino-Serrais et al., 2019). At least one image for each condition was acquired from each biological replicate.

### 2.7. PP2A activity assay

Cortico-hippocampal neurons were plated into 6-well plates. After treatments, cells were washed with PBS and detached in phosphatase storage buffer containing 5 mM EDTA, 2 mM ethyleneglycol-bis (β-aminoethyl)-N,N,N′,N′,-tetraacetic acid (EGTA), 0.5 mM phenylmethylsulfonyl fluoride (PMSF), 150 mM NaCl, 50 mM Tris-HCl pH 7.4, and 0.5 % protease inhibitor cocktail. Cells were sonicated at 20 kHz (ultrasonic) for 20 s on ice by a MICROSON Ultrasonic cell disruptor (MISONIX, Inc., Farmingdale, NY, USA) and centrifuged at 2000 *g* for 5 min at 4 °C. To remove free endogenous phosphate, the supernatant was passed through Sephadex G-25 spin columns; then, the activity of PP2A was measured using a Serine/Threonine Phosphatase Assay Kit (V2460, Promega) following the manufacturer's instructions. After protein quantification using the Pierce BCA Protein Assay Kit (Thermo Fisher Scientific), 1 μg of proteins was incubated with PP2A reaction buffer (250 mM imidazole pH 7.2, 1 mM EGTA, 0.1 % β-mercaptoethanol, and 0.5 mg/mL BSA) supplemented with Ser/Thr phosphopeptide in a 96-well plate (half area) for 30 min at 37 °C. The reaction was stopped by adding 50 μL of molybdate dye/additive mixture. After 15 min, the PP2A activity was measured at OD600 using a CLARIOstar plate reader (BMG LABTECH, Ortenberg, Germany).

### 2.8. Statistical analysis

Statistical analyses were performed using GraphPad Prism 10 software (GraphPad Software Inc., San Diego, CA, USA). Data were analyzed by using one-way ANOVA or two-way ANOVA followed by Bonferroni's multiple comparisons test. When comparing the two groups, the Mann-Whitney test was applied. All values are expressed as means ± standard deviation (SD), with individual data points presented. Each data point represents an independent biological replicate, which is denoted by 'n' in the figure legends. Three technical replicates were analyzed for each condition. Differences at $p < 0.05$ were considered statistically significant.

## 3. Results

### 3.1. OKA induces tau hyperphosphorylation in primary neurons

To obtain an AD-like *in vitro* model characterized by tauopathy, primary cultures of neurons isolated from *CYP46A1* overexpressing or WT embryos were incubated with OKA, a polyether toxin produced by different marine microalgae. OKA selectively inhibits tau dephosphorylation by PP2A, thus inducing hyperphosphorylated tau accumulation and aggregation, as demonstrated *in vivo* (Alvarez-de-la-Rosa et al., 2005; Zhang and Simpkins, 2010a) and *in vitro* (Zhang and Simpkins, 2010b) studies.

Before performing the experiments, the effects of OKA treatment on both cell viability and tau phosphorylation were investigated; primary neurons isolated from WT embryos were incubated with OKA at different concentrations (5, 10, 15, 20, 25 nM) for 6 h. According to LDH activity observed in the culture medium, OKA did not induce neuronal death at any of the tested concentrations (Supplementary Fig. 1A). By Western blotting, using the AT180 antibody, the effects of OKA on tau phosphorylation (at the Thr231 residue) were investigated. OKA promoted an increase in phosphorylated tau of approximately 3-fold ($p < 0.001$, $p < 0.0001$) at concentrations ranging from 10 to 25 nM (Supplementary Fig. 1B). Based on these data, for all experiments, the cells were incubated with OKA at the non-cytotoxic concentration of 10 nM.

### 3.2. Intracellular levels of 24-OHC are increased in both 24-OHC-treated wild type neurons and CYP46A1 overexpressing neurons

In a previous study performed by Shafaati and colleagues, brains from overexpressing human *CYP46A1* HA-tagged transgenic mice (CYP46Tg) showed ~2-fold enhanced production of 24-OHC compared to the brain of WT mice (Shafaati et al., 2011).

To also verify in our model the amount of the cerebral 24-OHC, the oxysterol quantification was performed in primary neurons isolated from WT or CYP46Tg embryos by GC–MS. In WT neurons, the oxysterol levels were investigated after incubation with 1 μM 24-OHC. Our findings show that 24-OHC levels are double ($p < 0.05$) in CYP46Tg neurons compared to control cells (WT neurons) (Fig. 2B); of note, in WT neurons incubated with the oxysterol, we observed a ~ 9.5-fold ($p < 0.05$) increase in 24-OHC content compared to control cells (Fig. 2A).

The evidence indicates that the overexpression of *CYP46A1* results in elevated oxysterol levels in comparison to normal WT neurons. Furthermore, after 24-OHC incubation, intraneuronal levels of 24-OHC significantly increased in WT neurons.

### 3.3. 24-OHC treatment and CYP46A1 overexpression prevent the hyperphosphorylation of tau in primary neurons

Tau hyperphosphorylation at Thr231 and Ser202/Thr205 residues

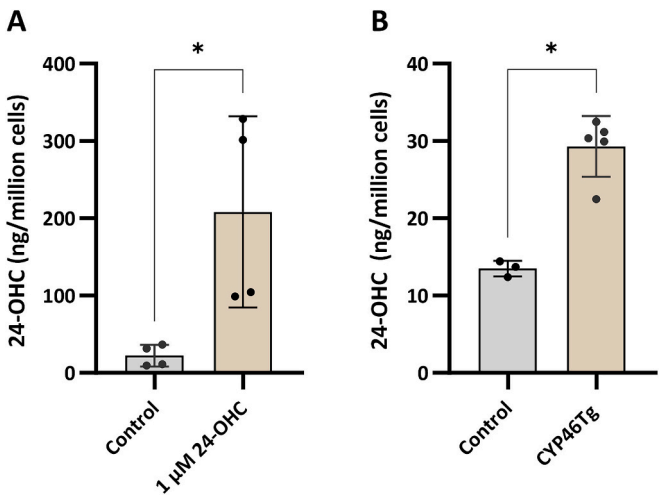


**Fig. 2.** Quantification of 24-OHC in primary neurons. The amount of 24-OHC was quantified by GC–MS: (A) in cortico-hippocampal neuronal primary cultures isolated from WT mice and incubated with or without 1 μM 24-OHC; the histograms represent mean values ± SD of two different experiments; (B) in cortico-hippocampal neuronal primary cultures isolated from CYP46Tg mice; the histograms represent mean values ± SD of two different experiments. *$p <$ 0.05 (Mann-Whitney test).

was investigated by Western blotting using AT180 antibody and AT8 antibody, respectively.

As shown in Fig. 3A, the incubation of WT neurons with OKA significantly induced the hyperphosphorylation of tau at Thr231 residue ($p < 0.0001$), compared to control cells. Concerning tau hyperphosphorylation at Ser202/Thr205 residues, although the phosphorylation was clearly increased by OKA, the data are not statistically significant. A similar trend has been observed in the cells treated with 24-OHC and OKA; the phosphorylation of both residues of tau is still higher compared to control cells but markedly lower compared to OKA treatment: the phosphorylation at Thr231 residue was significantly reduced ($p < 0.01$), while the phosphorylation at Ser202/Thr205 residues was decreased but not statistically significant. No significant changes were observed in cells incubated with 24-OHC compared to control cells. Concerning the *CYP46A1* overexpressing neurons, as reported in Fig. 3B, we found that OKA significantly increased tau phosphorylation only at Thr231 residue ($p < 0.05$) compared to control cells (WT neurons), but this increase was not significant compared to control CYP46Tg neurons. Instead, in WT neurons, OKA induced tau hyperphosphorylation at both residues ($p < 0.01$). Of note, the levels of phosphorylated tau at Thr231 and Ser202/Thr205 residues are lower in OKA-treated CYP46Tg neurons than in OKA-treated WT neurons, even if not statistically significant; moreover, tau phosphorylation levels at Thr231 residue remain significantly higher compared to control cells ($p < 0.05$), unlike those at Ser202/Thr205 residue. No significant changes were observed in total tau protein levels in both sets of experiments (Fig. 3A, B).

### 3.4. 24-OHC treatment and CYP46A1 overexpression prevent tau oligomer accumulation in primary neurons

Scientific evidence shows that the formation of NFTs alone is not sufficient to cause neurodegeneration; however, the prefibrillar tau oligomers have been demonstrated to be the most toxic form of tau, playing a key role in the pathology spreading, synaptic impairment, and cognitive decline in AD (Fá et al., 2016; Tai et al., 2014).

Using a specific T22 antibody against oligomeric tau, we observed a marked T22 immunoreactivity (~2.6 folds, $p < 0.0001$) in the soma of neurons treated with OKA compared to control cells, suggesting that OKA can promote tau oligomerization; of note, in neurons incubated with 1 μM 24-OHC and then with 10 nM OKA, tau oligomer accumulation was significantly prevented (~1.7 folds, $p < 0.0001$) compared to OKA treatment, although it remains slightly higher ($p < 0.05$) compared to control cells (Fig. 4A,B). Moreover, in Fig. 5A,B the hypothesis that *CYP46A1* overexpression may reduce the deposition of oligomeric tau species was also confirmed; after OKAinsult, CYP46Tg neurons display lower levels of T22 fluorescence intensity (~1.9 folds, $p < 0.01$) compared to OKA-treated WT neurons, pointing out that elevated 24-OHC prevents oligomeric tau formation.

### 3.5. 24-OHC treatment and CYP46A1 overexpression lead to partial prevention of morphology impairment in primary neurons

The cytoskeleton is a complex network of filaments that provides the cell with its shape and mechanical strength; the structural organization and dynamic remodeling of the cytoskeleton are particularly essential for neurons to develop axons and dendrites, establish synaptic connections, and ultimately ensure the transmission of electrical and chemical signals among neurons. Changes in the expression and stability of cytoskeletal proteins are indeed linked to several neurological disorders, including AD (Muñoz-Lasso et al., 2020).

The effects of 24-OHC treatment and *CYP46A1* overexpression on neuronal dendritic arborization were analyzed by confocal microscopy, evaluating the somatodendritic marker MAP2. As reported in Figs. 6A and 7A, the soma of primary neurons incubated with 10 nM OKA almost completely lost neuronal processes compared to control neurons, thus appearing with a rounded shape. Neuron pre-incubation with 1 μM 24-OHC partially prevented the impairment of the physiological structure of the cellular cytoskeleton (Fig. 6A). This beneficial effect of 24-OHC was also evident in CYP46Tg neurons, where the loss of neuronal processes was markedly prevented compared to WT neurons (Fig. 7A).

In addition, the entire dendritic tree of each cortico-hippocampal neuron was reconstructed in 3D by evaluating, as morphometric parameters, the number of intersections analyzed as a function of the distance from the soma and the dendritic length (Sholl Analysis). Our analysis indicates that WT neurons pre-incubated with 24-OHC, and then treated with OKA, significantly display a higher number of intersections compared to OKA-treated cells (Fig. 6B) as well as an increased dendritic length, although not significantly compared to cells incubated only with OKA (Fig. 6C). Moreover, overexpression of the enzyme CYP46A1 protects against OKA insult preserving both the number of intersections (Fig. 7B) and the dendritic length (Fig. 7C) compared to WT neurons incubated with OKA (~1.6 folds, $p < 0.05$).

### 3.6. CYP46A1 overexpression partially maintains PP2A activity in primary neurons

PP2A is a family of cellular key enzymes catalyzing the hydrolysis of phosphate esters at phospho-serine and phospho-threonine residues. PP2A accounts for approximately 70 % of tau phosphatase activity in the human brain, and a dysfunction in PP2A activity has been observed in AD brains (Sontag and Sontag, 2014).

We investigated whether 24-OHC treatment and *CYP46A1* overexpression could maintain PP2A activity in our OKA-induced tauopathy *in vitro* model. As reported in Fig. 8A, 10 nM OKA significantly blocks PP2A activity ($p < 0.001$) in WT neurons, underlying the possible involvement of PP2A inactivation in tau hyperphosphorylation, while the pre-incubation of neurons with 1 μM 24-OHC was not able to maintain significantly the PP2A activity. Concerning the results obtained in CYP46Tg neurons treated with OKA, interestingly, PP2A activity was not markedly blocked compared to control (WT neurons) and control CYP46Tg neurons, underlying a possible preservation of PP2A activity in these neurons. Indeed, after OKA insult, the activity of the enzyme appears higher in CYP46Tg neurons compared to WT ones, even if this difference is not statistically significant (Fig. 8B). The last data is in support of the previous finding (Fig. 3B), in which the

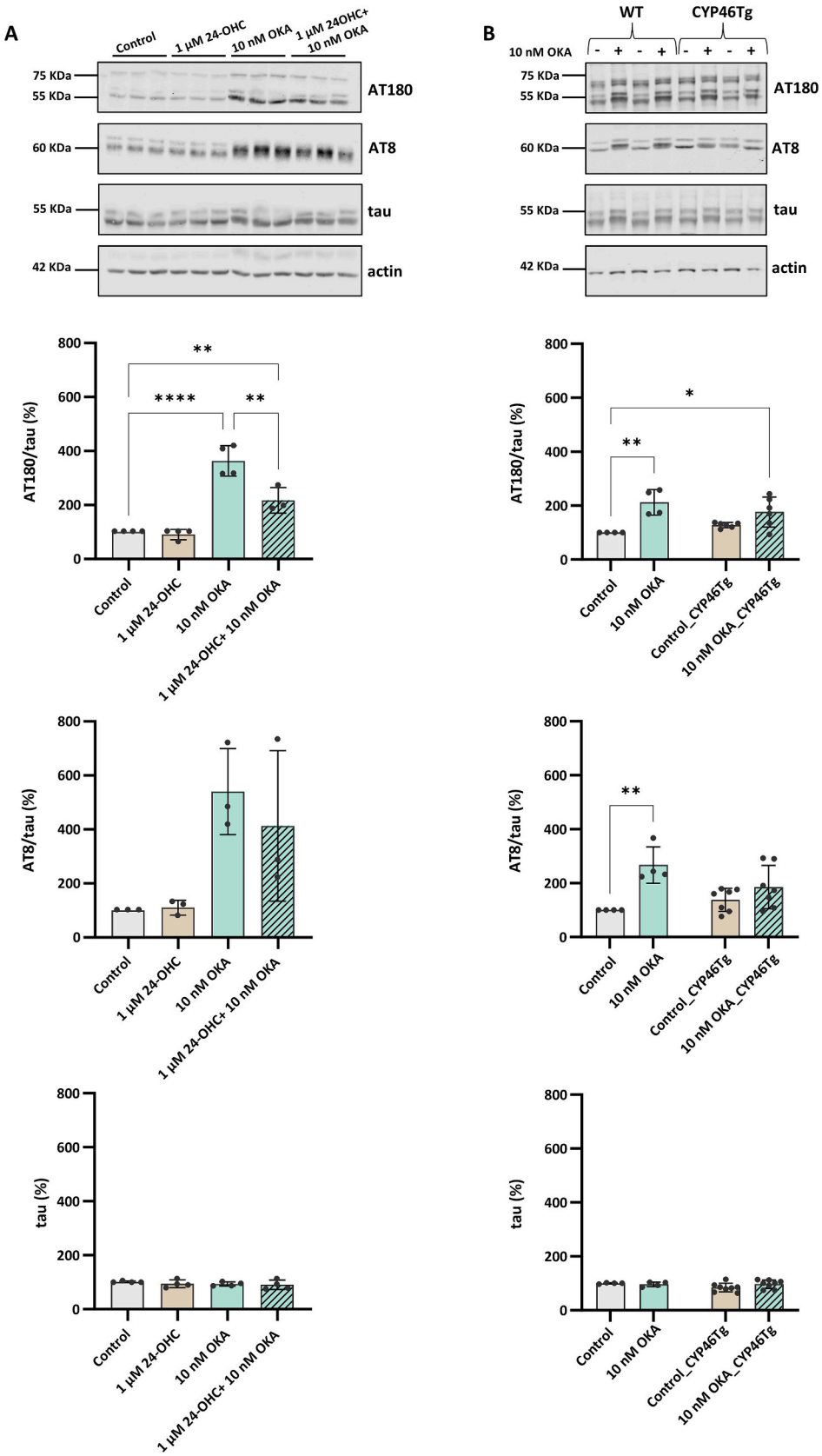


*(caption on next page)*

**Fig. 3.** Effects of 24-OHC treatment and CYP46A1 overexpression on tau hyperphosphorylation induced by OKA in primary neurons. (A) Cortico-hippocampal neuronal primary cultures isolated from WT mice were treated with or without 10 nM OKA in the presence or not of 1 μM 24-OHC. (B) Cortico-hippocampal neuronal primary cultures isolated from WT or CYP46Tg mice were treated with or without 10 nM OKA. The protein levels of phosphorylated tau at residues Thr231 or Ser202/Thr205 were analyzed by Western blotting, using AT180 and AT8 antibodies, respectively. Representative blots are shown. Phosphorylated tau densitometric measurements were normalized against the corresponding tau, which was first normalized to the corresponding actin levels. Data are expressed as a percentage of Control. (A) The histograms represent the mean values ± SD of four experiments for AT180 and three experiments for AT8. $^{**}p < 0.01$, $^{****}p < 0.0001$ (one-way ANOVA); (B) the histograms represent mean values ± SD of four experiments. $^{*}p < 0.05$, $^{**}p < 0.01$ (two-way ANOVA).

hyperphosphorylation of tau is lower in CYP46Tg neurons compared to WT neurons after OKA incubation.

### *3.7. Treatment with 24-OHC and the overexpression of CYP46A1 exert a neuroprotective effect, likely independent of tau kinases*

To elucidate the molecular mechanisms underlying the beneficial effects described above, we tested the involvement of the main Ser/Thr tau kinases, *i.e.*, ERK1/2, GSK3β, and CDK5.

ERK1/2, a member of the MAPK family, regulates multiple downstream processes (Albert-Gascó et al., 2020), including tau phosphorylation in both GSK3β-dependent and independent manner (Khezri et al., 2023).

As shown in Fig. 9A, OKA can activate ERK1/2 in WT neurons by stimulating its phosphorylation ($p < 0.05$); pre-incubation of cells with 24-OHC and then incubation with OKA slightly down-regulates ERK1/2 phosphorylation compared to cells only OKA-treated, although the levels remain high, but not statistically significant, compared to control cells. In Fig. 9B, results obtained in CYP46Tg neurons have been reported: ERK1/2 phosphorylation significantly increases after OKA treatment in CYP46Tg neurons *versus* control CYP46Tg ($p < 0.01$) and *versus* control (WT neurons) ($p < 0.001$). No significant modification in ERK1/2 levels was found in both sets of experiments (Fig. 9A, B).

GSK3β activity is increased in the brains of AD patients (Leroy et al., 2007), and GSK3β overexpression in mice results in tau hyperphosphorylation and AD-like tau pathology (Engel et al., 2006). Autophosphorylation on tyrosine-216 (Tyr216) mediates GSK3β activation, while phosphorylation on serine 9 (Ser9) by Akt, protein kinase A and B leads to its inhibition (Ly et al., 2013); additionally, dephosphorylation of Ser9 by protein phosphatases, including PP2A, directly activates GSK3β (Zhang et al., 2009).

In Supplementary Fig. 2A, OKA stimulates GSK3β phosphorylation at the Ser9 site in WT neurons compared to control cells. This increase is not statistically significant, but suggests a possible GSK3β inhibition. In neurons pre-incubated with 1 μM 24-OHC and then treated with 10 nM OKA, pSer9GSK3β levels remain higher than in control cells. As reported in Supplementary Fig. 2B, also CYP46Tg neurons treated with OKA show an increase of GSK3β phosphorylation at the Ser9 compared to control CYP46Tg neurons ($p < 0.001$) and *versus* control (WT neurons) ($p < 0.05$). We can hypothesize that the GSK3β inhibition is probably triggered by the blockage of PP2A activity caused by OKA; however, no significant changes in pTyr216GSK3β levels, the active form of the kinase, were observed in both cellular models, as well as in GSK3β ones. These data point out that 24-OHC effect is GSK3β-independent.

Various studies have shown a pivotal role of CDK5 in early synaptogenesis, normal dendritic spine retraction, and regulation of synaptic plasticity (Takahashi et al., 2022; Tanaka et al., 2022). The kinase activity of CDK5 depends on its binding with the subunit p35 and subsequent cytoplasmic membrane recruitment of the active complex CDK5/p35. In pathological conditions, when neurons suffer, the activation of $Ca^{2+}$-dependent protease calpain cleaves p35 to p25 (Kimura et al., 2014), which induces the hyperactivation of CDK5 (Patrick et al., 1999). In this connection, overexpression of the CDK5/p25 complex in neuroblastoma N2a cells induces tau hyperphosphorylation, resulting in impaired axonal transport (Zhou et al., 2010).

To investigate CDK5 modulation, a specific antibody that recognizes both p35 and p25 was used. In Supplementary Fig. 3A, OKA treatment, with or without the presence of 24-OHC, determines a significant reduction of p35 levels in WT neurons ($p < 0.001$), without affecting CDK5 expression. In Supplementary Fig. 3B, CYP46Tg neurons treated with OKA exhibited a lower level of p35 *versus* control CYP46Tg neurons ($p < 0.0001$) and *versus* control (WT neurons) ($p < 0.0001$), and this decrease is even lower compared to WT neurons treated with OKA ($p < 0.0001$). In both cellular models, we were not able to observe an increase in p25 levels following the p35 cleavage. Interestingly, in the absence of OKA, p35 levels were lower in CYP46Tg neurons compared to control ($p < 0.05$), suggesting a reduced basal expression of p35 in these neurons. Although we did not observe the accumulation of p25 in WT and CYP46Tg neurons, we cannot exclude CDK5 hyperactivation, since the p35 levels decreased in the OKA-treated neurons.

## 4. Discussion

It is now well accepted that during AD development various oxysterols, of enzymatic or not enzymatic origin, accumulate in the brain where they can act as friends or foes: most of these compounds have been shown to lead to neuron dysfunction and degeneration, contributing to neuroinflammation and amyloidogenesis (Gamba et al., 2011; Staurenghi et al., 2021; Testa et al., 2014; Yamanaka et al., 2011). On the other hand, certain oxysterols, such as 24-OHC, may provide neuroprotective benefits. However, the exact molecular mechanisms, especially those responsible for these protective effects, remain to be clarified.

The main oxysterol present in the healthy brain is 24-OHC, also named cerebrosterol, and considerable evidence shows that it represents a molecule of great importance for physiological brain functions. Indeed, 24-OHC plays a vital role in maintaining the brain cholesterol homeostasis by regulating the feedback loop between astrocytes and neurons, ensuring both the availability of cholesterol for neuronal uptake and the removal of excess cholesterol (Abildayeva et al., 2006). Based on the detailed overview of Gamba and colleagues, 24-OHC appears to have a controversial role in AD pathogenesis due to its ability to exert both detrimental and beneficial effects (Gamba et al., 2021); for instance, as regards its neuroprotective roles, it has been demonstrated to induce an adaptive response (Okabe et al., 2013), to suppress amyloid β (Aβ) accumulation in the brain (Prasanthi et al., 2009; Urano et al., 2013), and to support synaptic plasticity and function in rat hippocampal neurons and slices by amplifying responses through *N*-methyl-D-aspartate receptors (NMDARs) (Linsenbardt et al., 2014; Paul et al., 2013). In addition, it has been demonstrated by our group that 24-OHC modulates the expression and synthesis of the deacetylase SIRT1 in SK-N-BE neuroblastoma cells, which, in turn, prevents tau phosphorylation and promotes its deacetylation, making tau more susceptible to proteasomal degradation (Testa et al., 2023; Testa et al., 2018). The neuroprotective effect of 24-OHC was robustly demonstrated through *in vivo* experiments: a four-day pre-treatment with 24-OHC administered to hTau mice through intracerebroventricular injections fully blocked tau hyperphosphorylation triggered by Aβ injection in the brain of these mice (Testa et al., 2018). Given the fact that 24-OHC loss could contribute to accelerated AD progression, a significant decline in 24-OHC content and *CYP46A1* gene expression has been observed in the frontal and occipital cortices of *post-mortem* human AD brains at advanced stages of tau pathology (Testa et al., 2016). CYP46A1 influences at least three key processes in the brain: sterol flux through the plasma membrane, acetyl-CoA production, and mevalonate synthesis in the cholesterol biosynthesis pathway. These primary effects, in turn,

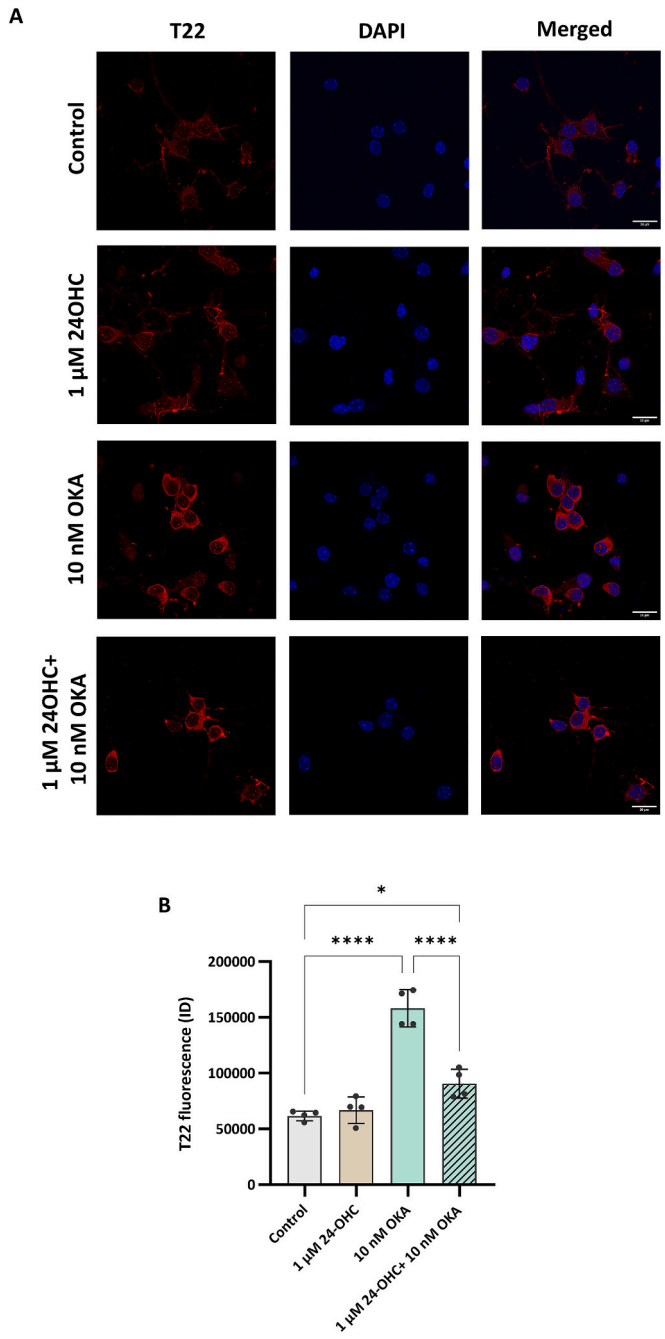


**Fig. 4.** Effects of 24-OHC treatment on intracellular accumulation of tau oligomers induced by OKA in primary neurons. Cortico-hippocampal neuronal primary cultures isolated from WT mice were treated with or without 10 nM OKA in the presence or not of 1 µM 24-OHC. (A) Tau oligomer levels were analyzed by immunocytochemistry using the T22 antibody (red). Nuclei were stained with DAPI (blue). Representative images of two different experiments are shown. Cells were imaged using an LSM900-Airy confocal laser microscope (Zeiss, 63× oil immersion objective; scale bar: 20 µm). (B) T22 fluorescence intensity, analyzed by Fiji ImageJ, was expressed as the average of the integrated density (ID) quantified in the soma of each neuron (number of neurons = 5–12 per image). The histograms represent the mean values ± SD of two experiments. *$p < 0.05$, ****$p < 0.0001$ (one-way ANOVA). (For interpretation of the references to colour in this figure legend, the reader is referred to the web version of this article.)

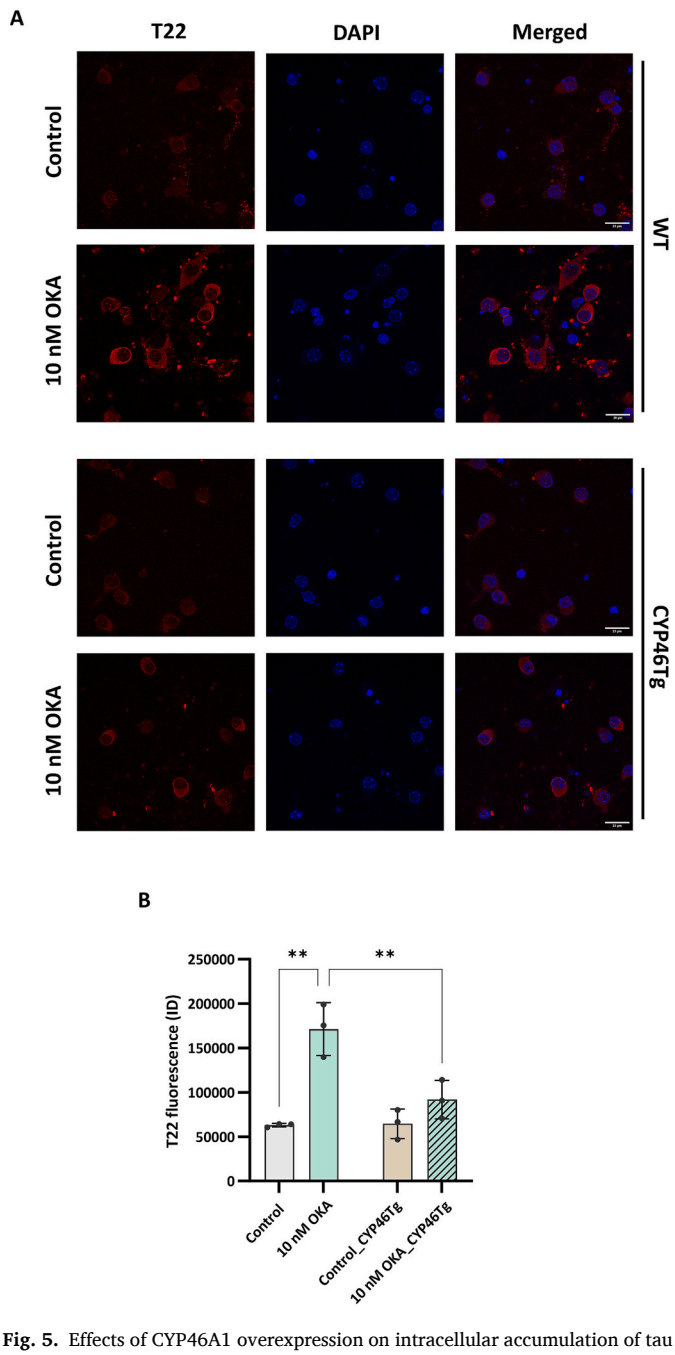


**Fig. 5.** Effects of CYP46A1 overexpression on intracellular accumulation of tau oligomers induced by OKA in primary neurons. Cortico-hippocampal neuronal primary cultures isolated from WT or CYP46Tg mice were treated with or without 10 nM OKA. (A) Tau oligomer levels were analyzed by immunocytochemistry using the T22 antibody (red). Nuclei were stained with DAPI (blue). Representative images of two different experiments are shown. Cells were imaged using an LSM900-Airy confocal laser microscope (Zeiss, 63× oil immersion objective; scale bar: 20 µm). (B) T22 fluorescence intensity, analyzed by Fiji ImageJ, was expressed as the average of the integrated density (ID) quantified in the soma of each neuron (number of neurons =4–14 per image). The histograms represent the mean values ± SD of one experiment. **$p < 0.01$ (two-way ANOVA). (For interpretation of the references to colour in this figure legend, the reader is referred to the web version of this article.)

impact various secondary processes, including cholesterol content in lipid rafts and physicochemical properties of plasma membranes (Boussicault et al., 2018), long-term potentiation (Mitroi et al., 2019; Popiolek et al., 2020), motor functions (Boussicault et al., 2016), autophagy and lysosomal function (Ayciriex et al., 2017; Nóbrega et al., 2019), protein phosphorylation, synaptic glutamate release, and acetylcholine biosynthesis (Mast et al., 2021; Petrov et al., 2020).

Despite these findings, the connection between 24-OHC and tau

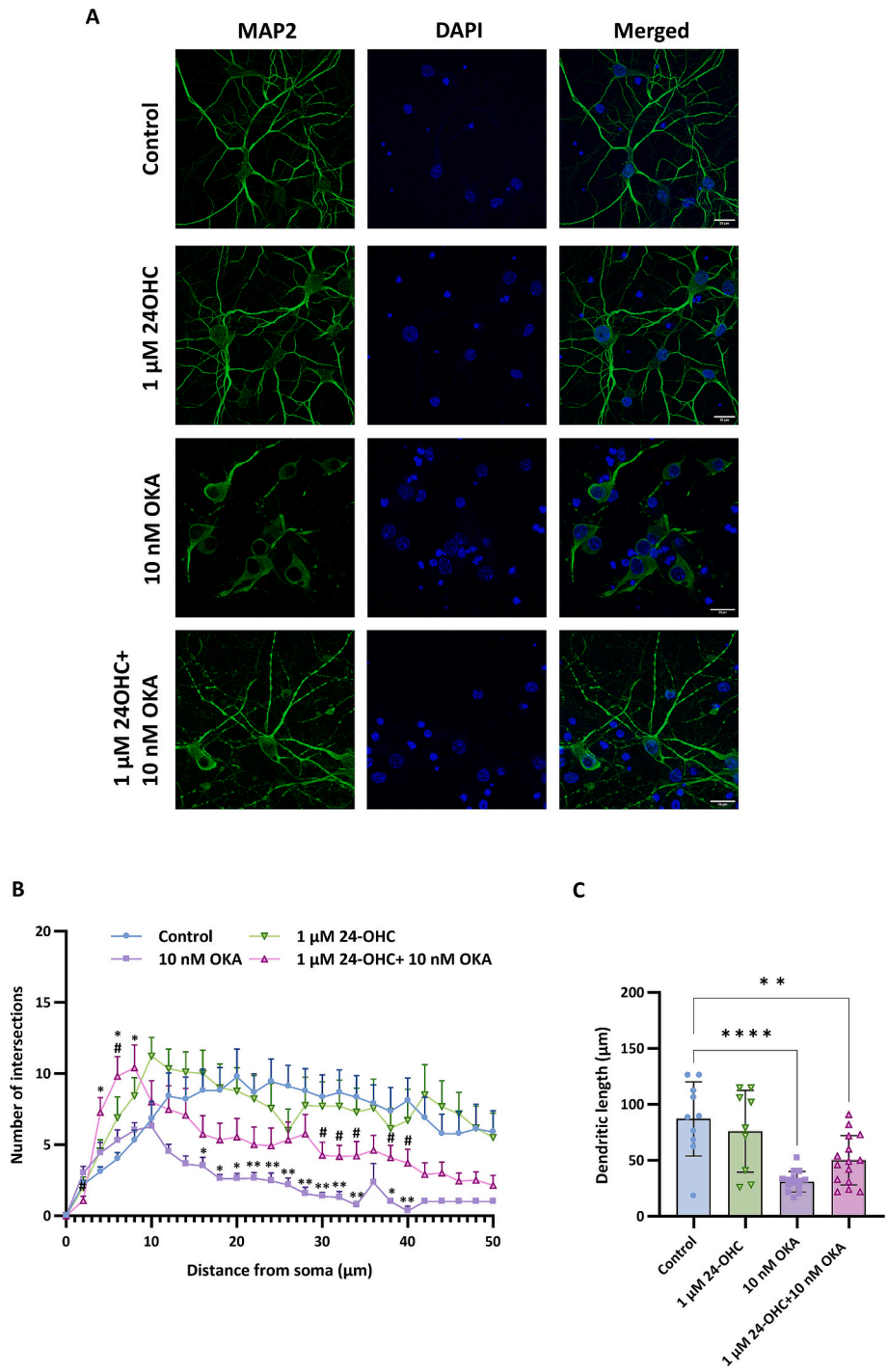


**Fig. 6.** Effects of 24-OHC treatment on neuronal morphology impairment induced by OKA in primary neurons. Cortico-hippocampal neuronal primary cultures isolated from WT mice were treated with or without 10 nM OKA in the presence or not of 1 μM 24-OHC. (A) Neuronal morphology was analyzed by immunocytochemistry using MAP2 antibody (green). Nuclei were stained with DAPI (blue). Representative images of two different experiments are shown. Cells were imaged using an LSM900-Airy confocal laser microscope (Zeiss, 63× oil immersion objective; scale bar: 20 μm). (B,C) Sholl analysis was performed by Imaris software, measuring two different morphometric parameters: (B) the number of intersections was expressed as a function of the distance from the soma (from 1 to 50 μm radii). The graphs represent mean values ± SD of two different experiments (number of neurons = 9–15 per treatment group). 10 nM OKA *vs* Control: $*p < 0.05$ at 16–21, 31, 37, 38, 39 μm, $**p < 0.01$ at 22–30, 32–35, 40 μm; 1 μM 24-OHC + 10 nM OKA *vs* Control: $*p < 0.05$ at 4, 5, 6, 7, 8 μm; 1 μM 24-OHC + 10 nM OKA *vs* 10 nM OKA; $\#p < 0.05$ at 2, 5, 6, 7, 30, 32, 33, 34, 37, 38, 39, 40 μm (two-way ANOVA); (C) the dendritic length was calculated per each neuron as the distance from the soma. The histogram represents mean values ± SD of two different experiments (number of neurons = 9–15 per treatment group). $**p < 0.01$, $****p < 0.0001$ (one-way ANOVA). (For interpretation of the references to colour in this figure legend, the reader is referred to the web version of this article.)

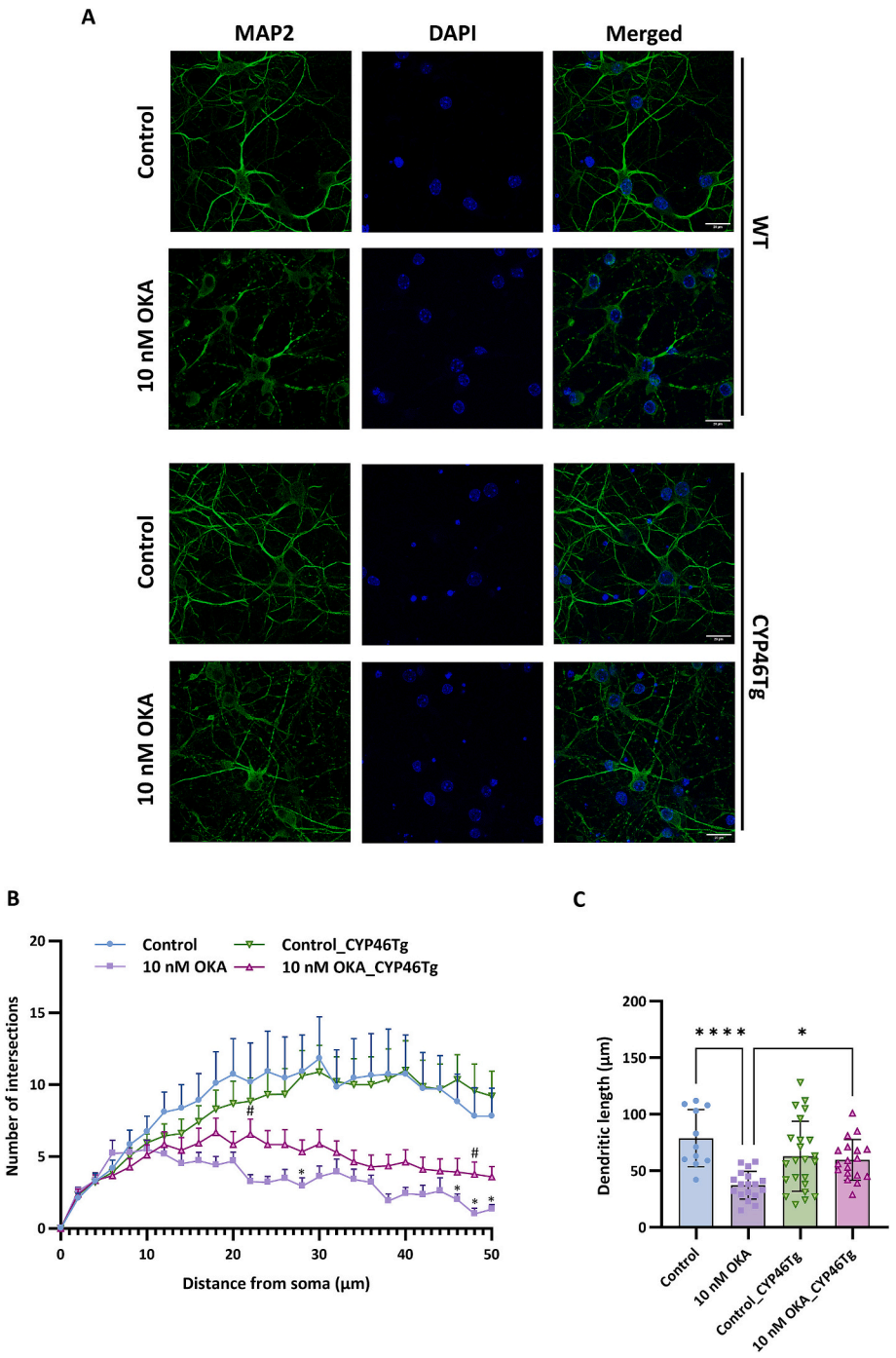


**Fig. 7.** Effects of CYP46A1 overexpression on neuronal morphology impairment induced by OKA in primary neurons. Cortico-hippocampal neuronal primary cultures isolated from WT or CYP46Tg mice were treated with or without 10 nM OKA. (A) Neuronal morphology was analyzed by immunocytochemistry using MAP2 antibody (green). Nuclei were stained with DAPI (blue). Representative images of two different experiments are shown. Cells were imaged using an LSM900-Airy confocal laser microscope (Zeiss, 63× oil immersion objective; scale bar: 20 µm). (B,C) Sholl analysis was performed by Imaris software, measuring two different morphometric parameters: (B) the number of intersections was expressed as a function of the distance from the soma (from 1 to 50 µm radii). The graphs represent mean values ± SD of two different experiments (number of neurons = 11–23 per treatment group). 10 nM OKA *vs* Control: $*p < 0.05$ at 28, 43, 46, 47–50 µm; 10 nM OKA_CYP46Tg *vs* 10 nM OKA: $\#p < 0.05$ at 1, 22, 23, 47, 48 µm (two-way ANOVA); (C) the dendritic length was calculated per each neuron as the distance from the soma. The histogram represents mean values ± SD of two different experiments (number of neurons = 11–23 per treatment group). $*p < 0.05$, $****p < 0.0001$ (one-way ANOVA). (For interpretation of the references to colour in this figure legend, the reader is referred to the web version of this article.)

pathology, along with NFT formation, is still not completely understood. The present research aims to investigate whether maintaining high levels of 24-OHC in neurons, through exogenous administration of 24-OHC or *CYP46A1* overexpression, counteracts tau deposits in the OKA-induced *in vitro* model. The *CYP46A1* overexpressing neurons were isolated from CYP46Tg mice generated for the first time by Shafaati and collaborators. In this animal model, expressing the human *CYP46A1* gene, the levels of CYP46A1 enzyme are estimated to be about 10-fold higher in the brain than in the other organs (*i.e.*, eye, liver, lung, kidney, ovary, and testis); consequently, there was a significant increase in the brain and plasma content of 24-OHC, respectively two and five folds compared to WT mice (Shafaati et al., 2011).

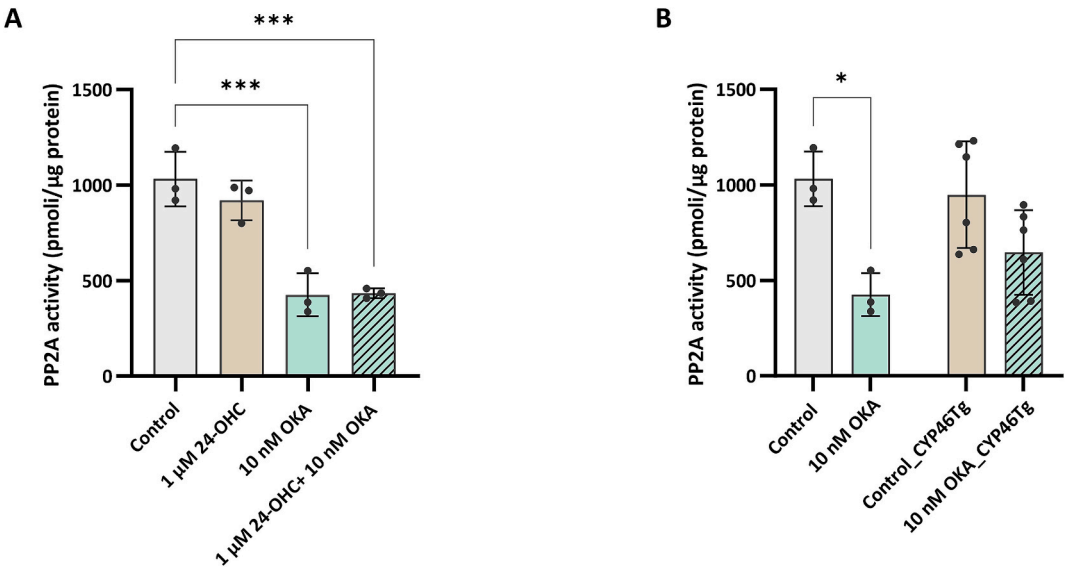


**Fig. 8.** Effect of 24-OHC treatment and CYP46A1 overexpression on PP2A activity in primary neurons. (A) Cortico-hippocampal neuronal primary cultures isolated from WT mice were treated with or without 10 nM OKA in the presence or not of 1 µM 24-OHC. (B) Cortico-hippocampal neuronal primary cultures isolated from WT or CYP46Tg mice were treated with or without 10 nM OKA. PP2A activity was analyzed by a Serine/Threonine Phosphatase Assay Kit. The histograms represent the mean values ± SD of three experiments. (A) $^{***}p < 0.001$ (one-way ANOVA). (B) $^{*}p < 0.05$ (two-way ANOVA).

Our data show that the incubation of neurons with 24-OHC can counteract tau hyperphosphorylation, mainly at Thr231 residue (Fig. 3A,B). In the current study, the amount of 24-OHC was quantified in both WT neurons incubated with 1 µM 24-OHC and in CYP46Tg neurons; although the levels of the oxysterol were seven times lower in the CYP46Tg neurons (Fig. 2B) compared to WT neurons incubated with 24-OHC (Fig. 2A), the prevention of tau hyperphosphorylation in the transgenic neurons was consistent. Of note, the amount of 24-OHC in *CYP46A1* overexpressing neurons was twice as high as that of WT neurons (control).

We can hypothesize that the higher levels of 24-OHC in primary neurons reduce tau protein levels, presumably due to tau-increased proteasomal degradation, as demonstrated in our recent publication; indeed, the 24-OHC was found to induce ubiquitin-proteasome system (UPS)-dependent tau clearance, by acting on the SIRT1/peroxisome proliferator-activated receptor gamma coactivator 1-alpha (PGC1α)/Nuclear factor erythroid 2-related factor 2 (Nrf2) pathway (Testa et al., 2023). In this connection, to support the beneficial role of 24-OHC, an interesting study exploring the association between the levels of 24-OHC in cerebrospinal fluid (CSF) and neurodegeneration biomarkers has been conducted. In a clinical cohort of subjective cognitive impairment (SCI), mild cognitive impairment (MCI), and AD patients, the authors observed that higher levels of 24-OHC correlate with lower levels of phosphorylated tau and total tau in all three cohorts but only in women (Latorre-Leal et al., 2024). In other studies, astrocytes and neurons, deriving from familial AD-patient induced pluripotent stem cells (iPSC), were incubated with the anti-HIV drug Efavirenz (EFV), an allosteric activator of the CYP46A1 enzyme; EFV treatment reduced the accumulation of phosphorylated tau in neurons and enhanced the turnover of cholesterol to 24-OHC by the conversion of cholesteryl esters (CE) to cholesterol. This reduction of CE leads to proteasome upregulation and degradation of phosphorylated tau (van der Kant et al., 2020; van der Kant et al., 2019). On the other hand, a raised cholesterol metabolism could damagingly sustain tau seeding. Indeed, Tuck and colleagues demonstrated, in primary neurons, that cholesterol depletion from the plasma membrane using the cholesterol-extracting agent methyl-beta-cyclodextrin (MβCD), as well as treatment with 24-OHC or EFV, busted tau entrance (Tuck et al., 2022).

Mast and colleagues have extensively expanded their knowledge on the wide-ranging effects of CYP46A1 activity modulation in the brain of mice treated with EFV; changes in the regulation of different processes, including not only cholesterol homeostasis, metabolism of lipids, carbohydrates, and amino acids, neuroprotection, synaptic function, inflammation, and apoptosis but also autophagy and UPS events, were detected in *CYP46A1*$^{-/-}$ mice (Mast et al., 2017a) and EFV-treated 5XFAD mice (Mast et al., 2024; Mast et al., 2020). Moreover, endosomal-lysosomal membrane trafficking was impaired in mice with decreased hippocampal *CYP46A1* expression (Ayciriex et al., 2017). This evidence further suggests that increased activity of CYP46A1 could reduce tau accumulation and the consequent formation of NFTs by favoring its clearance through protein degradation machinery.

Augustinack and colleagues defined 3 stages of NFTs: 1) the pre-neurofibrillary tangles (pre-NFTs) state, characterized by non-fibrillar punctate regions in the cytoplasm of neurons that include sound dendrites and somas, as observed especially with antibodies against phosphorylated tau at Thr231, Ser262, and Thr153 residues. The nucleus is discernible and the overall cellular morphology appears normal; 2) intraneuronal neurofibrillary tangles (iNFTs) that exhibit homogeneous staining with fibrillar tau structures, prominently labelled by antibodies recognizing tau phosphorylation at Thr175/181, 12E8 (Ser262/Ser356), Ser422, Ser46, and Ser214. The nucleus is present but often eccentric or pyknotic; 3) extracellular neurofibrillary tangles (eNFTs) containing filaments of phosphorylated tau that are stained by AT8 (Ser199/Ser202/Thr205), AT100 (Thr212/Ser214), and PHF-1 (Ser396/Ser404) antibodies, which also stain iNFTs; these filaments resembling neuronal cell bodies are also referred to as “ghost tangles” (Augustinack et al., 2002). Mainly based on the third stage, a characteristic of pathological tau is the propagation of tau fibrils between neurons, thus spreading to distant brain regions in a prion-like manner (Spillantini and Goedert, 2013). Indeed, eNFTs, mainly in the shape of tau oligomers, enter cells *via* endocytosis and promote the recruitment of soluble tau into growing aggregates. Some of them are released and taken up by healthy cells, initiating another cycle of seeded fibrillization (Frost et al., 2009; Guo and Lee, 2013; Wu et al., 2013). Tau pathological cell-to-cell transmission is a critical event at the basis of AD progression. In this regard, detecting phosphorylated oligomeric tau species in cortical synapses from AD brains (Henkins et al., 2012) suggests that highly phosphorylated tau multimers contribute to tau transmission and related neuronal dysfunction. In particular, tau oligomeric forms affect several intraneuronal processes, including microtubule assembly,

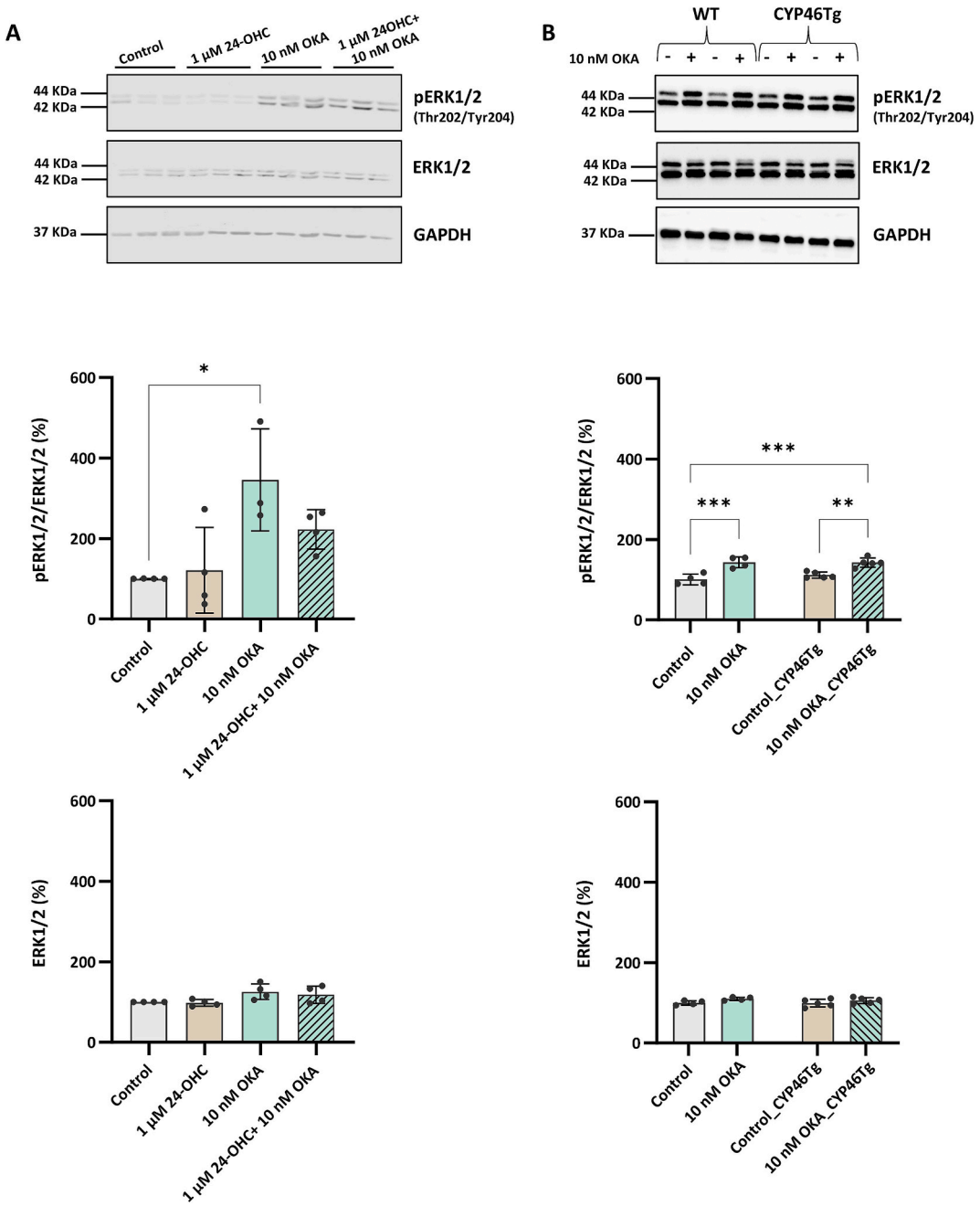


**Fig. 9.** Effects of 24-OHC treatment and CYP46A1 overexpression on ERK1/2 kinase activation in primary neurons. (A) Cortico-hippocampal neuronal primary cultures isolated from WT mice were treated with or without 10 nM OKA in the presence or not of 1 μM 24-OHC. (B) Cortico-hippocampal neuronal primary cultures isolated from WT or CYP46Tg mice were treated with or without 10 nM OKA. The protein levels of phosphorylated ERK1/2 at Thr202/Tyr204 residue and ERK1/2 were analyzed by Western blotting. Representative blots are shown. Phosphorylated ERK1/2 densitometric measurements were normalized against the corresponding ERK1/2, which was first normalized to the corresponding actin levels. Data are expressed as a percentage of Control. The histograms represent the mean values ± SD of (A) three experiments, $*p < 0.05$ (one-way ANOVA), or of (B) two experiments, $**p < 0.01$, $***p < 0.001$ (two-way ANOVA).

neuronal cytoskeleton, and axonal transport (Niewiadomska et al., 2021).

In the present study, we investigated whether the increase of 24-OHC levels could reduce tau oligomer accumulation in neurons, due to its capability to prevent phosphorylation of tau (Fig. 3). For the first time, we demonstrated that the preincubation of WT neurons with 24-OHC can prevent the accumulation of tau oligomers upon OKA treatment (Fig. 4A,B). Similarly, in the *CYP46A1* overexpressing neurons, the endogenous production of 24-OHC was also able to counteract tau oligomerization (Fig. 5A,B).

Modifications in the structure of dendritic spines, which are essential for memory, learning, and cognitive functions, have been linked to AD pathology (Knafo et al., 2009), and the progressive atrophy of dendrites is associated with the accumulation of tau aggregates (Merino-Serrais et al., 2013). As previously observed by Arias and co-workers, OKA increases the phosphorylation of MAP2, affecting the organization and stability of the neuronal cytoskeleton (Arias et al., 1993). Our data demonstrated that both 24-OHC treatment and the overexpression of *CYP46A1* partially prevented the neuronal architecture impairment induced by OKA treatment (Figs. 6 and 7). These data are in agreement with other studies reporting that CYP46A1 regulates different proteins involved in the cytoskeletal arrangement, such as MAP2, centrosomal

protein 170B (CEP170B), microtubule-associated protein 1B (MAP1B), dihydropyrimidinase like 2 (DPYSL2), catenin delta 2 (CTNND2), growth-associated protein 43 (GAP43), and neurofilament heavy chain (NEFH) (Mast et al., 2021; Petrov et al., 2020). The cytoskeleton may play a critical role in synaptic plasticity (Gordon-Weeks and Fournier, 2014). As demonstrated by Maioli and colleagues, the levels of presynaptic and postsynaptic proteins, such as synaptophysin, synapsin-1, postsynaptic density 9 (PSD95), NMDAR1, and p-NMDAR2A, were significantly increased in the hippocampus of the *CYP46A1* transgenic mice as compared to the control mice. As a consequence of the up-regulation of these markers, an improvement in spatial memory was observed (Maioli et al., 2013). Moreover, 24-OHC was found to be a positive allosteric modulator of the glutamate NMDAR subunit epsilon-2 (GluN2B) of NMDAR (Paul et al., 2013; Wei et al., 2019).

Previous findings, obtained by Petrov and co-workers, pointed out that CYP46A1 stimulation in EFV-treated 5XFAD mice modulates the activity either of several kinases involved in tau phosphorylation (*e.g.*, CDK5, casein kinase 1/2, GSK3α/β, and p38 MAPK) or of protein phosphatases able to dephosphorylate tau (*e.g.*, PP1/2A and PP2B) (Petrov et al., 2019).

Based on this evidence, we decided to analyze tau kinase levels and phosphatase activity to investigate the molecular mechanisms through which the oxysterol 24-OHC could exert its neuroprotective effects in reducing tau phosphorylation. Although the data obtained are not clear, in the *in vitro* model of tauopathy employed in this paper, OKA seems able to induce tau hyperphosphorylation not only through the inhibition of PP2A activity (Fig. 8A,B), but also through ERK1/2 phosphorylation (Fig. 9A,B). Notably, in CYP46Tg neurons treated with OKA, the inhibition of PP2A seems to be mostly prevented (Fig. 8B), according to the data reported by Petrov and co-workers (Petrov et al., 2019).

There was no evidence of PP2A activity prevention in 24-OHC-treated neurons after OKA insult (Fig. 8A), suggesting that this effect could be a consequence of the modulation of CYP46A1-dependent pathways. In contrast to other studies in which OKA was able to stimulate the main kinases involved in tau phosphorylation (*i.e.*, ERK1/2, GSK3β, and CDK5) (Chou and Yang, 2021; Huang et al., 2019), in our *in vitro* model we only found an increase in ERK1/2 phosphorylation at Thr202 and Tyr204 (active form). Other studies have also demonstrated, in different regions of the AD brain, an association between elevated levels of phosphorylated ERK1/2 at residues Thr202/Tyr204 and tau phosphorylation and early neurofibrillary degeneration (Ferrer et al., 2001; Pei et al., 2002). Given that PP2A dephosphorylates ERK1/2 (Khezri et al., 2023), we can presume that ERK1/2 phosphorylation increased as a result of the inhibition of PP2A activity. To confirm this hypothesis, a previous study found that the inhibition of cellular phosphatase PP2A by hesperetin maintains the activation status of ERK1/2 in cortical neurons (Vauzour et al., 2018).

GSK3β, ubiquitously expressed and constitutively active, takes part in numerous key cellular signaling pathways, including neurodegeneration processes. In particular, GSK3β activity is increased in the brains of AD patients (Leroy et al., 2007), and its overexpression in mice results in tau hyperphosphorylation and AD-like tau pathology (Engel et al., 2006). GSK3β exists in active and inactive forms depending on its phosphorylation status. Auto-phosphorylation on the tyrosine-216 (Tyr216) site mediates its activation, while phosphorylation on the serine 9 (Ser9) site leads to its inhibition (Ly et al., 2013); additionally, dephosphorylation of Ser9 by PP1/2A/2B directly activates GSK3β (Zhang et al., 2009). Based on our results, phosphorylation of GSK3β at the Ser9 site (inactive form) increased after OKA treatment (Supplementary Fig. 2A,B), most likely following PP2A activity blockage. Of note, Kim and colleagues reported that by blocking GSK3β with its inhibitor TDZD-8, the phosphorylation of GSK3β at the Ser9 site was induced, triggering the increase of ERK1/2 phosphorylation (Kim et al., 2007). Based on this study, we can suppose that GSK3β inhibition could also be involved in ERK1/2 activation; in turn, ERK1/2 could drive tau phosphorylation in a GSK3β-independent manner; in fact, we did not observe a rise in its phosphorylation at the Tyr216 site.

The kinase activity of CDK5 is determined by its binding with the subunit p35 and subsequent cytoplasmic membrane recruitment of the active complex CDK5-p35. Physiologically, p35 is an unstable protein with a short life span and is degraded by UPS. In pathological conditions, when neurons suffer from stress, death signals, or overexcitation, large influxes of $Ca^{2+}$ enter the cytoplasm, triggering the activation of $Ca^{2+}$-dependent protease calpain, which cleaves p35 to p25 (Kimura et al., 2014). The subunit p25 displays a longer half-life, and this results in hyperactivation of CDK5 (Patrick et al., 1999). A significantly higher p25/p35 ratio was observed in *post-mortem* human AD brains (Tseng et al., 2002), and the overexpression of the CDK5-p25 complex in neuroblastoma N2a cells was able to induce tau hyperphosphorylation, resulting in impaired axonal transport (Zhou et al., 2010). In cerebral organoids derived from induced iPSCs carrying the tau P301L mutation, the blocking of p25 generation reduced the levels of phosphorylated tau while elevated synaptophysin expression (Seo et al., 2017). In the present work, OKA was found to reduce p35 levels in WT and CYP46A1 neurons, but this decrease is not matched by p25 accumulation (Supplementary Fig. 3A,B), which could indicate a CDK5 hyperfunctionality. Despite that, we cannot exclude that p35 is cleaved into p25; p35 decrease is more enhanced in *CYP46A1* overexpressing neurons after OKA treatment (Supplementary Fig. 3B); this result could suggest that the CYP46A1 enzyme might affect CDK5 activation.

Although it is clear that elevated levels of 24-OHC exert protective effects against OKA-induced tau hyperphosphorylation and neuronal morphology impairment, we did not obtain evidence on the underlying molecular mechanisms involved, emphasizing the need to study these aspects further. However, we should keep in mind that *CYP46A1* overexpression and 24-OHC treatment could enhance neuroprotection through other mechanisms; for example, an enhancement of spatial memory and dendritic spine length and area was shown in older female mice overexpressing *CYP46A1* through indirect activation of estrogen receptor (ER) signaling in the hippocampus. This result was further confirmed in hippocampal neurons, where 24-OHC treatment leads to nuclear translocation and up-regulation of ER and its downstream target genes, such as activity-regulated cytoskeletal protein (*Arc*), a gene involved in learning and memory and believed to play an integral role in synapse-specific plasticity (Latorre-Leal et al., 2024).

## 5. Conclusions

The anti-neurodegenerative effects of 24-OHC treatment and *CYP46A1* overexpression on primary neurons are summarized in Fig. 10.

Our study suggests that preventing 24-OHC loss in the brain could be a promising strategy to counteract tau phosphorylation and the consequent tau oligomerization and, eventually, tau propagation in the AD brain, preserving the integrity of the neuronal morphology. At the same time, the limitation of this research is represented by the fact that the underlying molecular mechanisms remain unclear, particularly those relating to the action of 24-OHC. However, our results encourage more in-depth investigations on cellular tau secretion, propagation, and uptake mechanisms, confirming the potential of CYP46A1-targeting pharmacological approaches, such as with the use of activators of the CYP46A1 enzyme, to maintain high levels of 24-OHC to counteract AD progression.

Supplementary data to this article can be found online at https://doi.org/10.1016/j.nbd.2025.107029.

## CRediT authorship contribution statement

**Serena Giannelli:** Writing – original draft, Visualization, Methodology, Investigation, Funding acquisition, Formal analysis, Conceptualization. **Francesca Eroli:** Funding acquisition, Formal analysis. **Raúl Loera-Valencia:** Methodology, Investigation. **Valerio Leoni:** Methodology, Investigation. **Maria Latorre-Leal:** Methodology, Funding

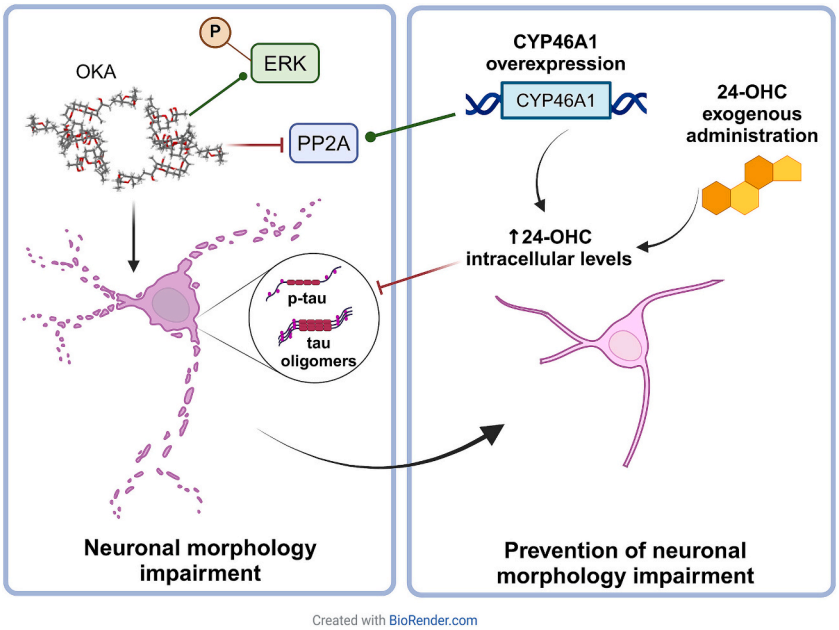


**Fig. 10.** The beneficial effects of 24-OHC treatment and CYP46A1 overexpression on primary neurons are summarized (created with BioRender.com).

acquisition. **Gabriella Testa:** Funding acquisition. **Erica Staurenghi:** Methodology. **Barbara Sottero:** Visualization. **Paola Gamba:** Writing – review & editing. **Silvia Maioli:** Writing – review & editing, Supervision, Resources, Funding acquisition, Conceptualization. **Gabriella Leonarduzzi:** Writing – review & editing, Supervision, Resources, Funding acquisition, Conceptualization.

## Ethical statement

All experimental procedures on mice were performed following the local national animal care and guidelines and approved by the local committee of Karolinska Institutet and the Swedish Board of Agriculture (ethical permit ID 4884/2019). All possible efforts were made to minimize the suffering and distress of the animals.

## Funding

This work was supported by C.M. Lerici Foundation (S.G.); The Foundation Blanceflor (S.G.); Gun och Bertil Stohnes Stiftelse (S.G., S. M., F.E., M.L.-L.); Stiftelsen Gamla Tjänarinnor (SM, FE, ML-L); Margaretha af Ugglas' Foundation (S.M., F.E., M.L.-L.); King Gustaf V and Queen Victoria's Foundation (S.M.); "Innovative ways to fight Alzheimer's disease - Leif Lundblad Family and others" (S.M.); Swedish Research Council (2024-03440) (S.M.); Alzheimerfonden (AF-1011030) (S.M.); Olle Engqvists (231-0067) (S.M.); Grant for internationalization (TESG_GFI_22_01_F) (G.T.); University of Turin (LEOG_RILO_22_01, LEOG_RILO_23_01) (G.L.).

## Declaration of competing interest

The authors declare no conflict of interest.

## Data availability

Data will be made available on request.

## References

Abildayeva, K., Jansen, P.J., Hirsch-Reinshagen, V., Bloks, V.W., Bakker, A.H., Ramaekers, F.C., Mulder, M., 2006. 24(S)-hydroxycholesterol participates in a liver X receptor-controlled pathway in astrocytes that regulates apolipoprotein E-mediated cholesterol efflux. J. Biol. Chem. 281 (18), 12799–12808. https://doi.org/10.1074/jbc.M601019200.

Ahmed, H., Wang, Y., Griffiths, W.J., Levey, A.I., Pikuleva, I., Liang, S.H., Haider, A., 2024. Brain cholesterol and Alzheimer's disease: challenges and opportunities in probe and drug development. Brain 147 (5), 1622–1635. https://doi.org/10.1093/brain/awae028.

Albert-Gascó, H., Ros-Bernal, F., Castillo-Gómez, E., Olucha-Bordonau, F.E., 2020. MAP/ERK signaling in developing cognitive and emotional function and its effect on pathological and neurodegenerative processes. Int. J. Mol. Sci. 21 (12). https://doi.org/10.3390/ijms21124471.

Alvarez-de-la-Rosa, M., Silva, I., Nilsen, J., Pérez, M.M., García-Segura, L.M., Avila, J., Naftolin, F., 2005. Estradiol prevents neural tau hyperphosphorylation characteristic of Alzheimer's disease. Ann. N. Y. Acad. Sci. 1052, 210–224. https://doi.org/10.1196/annals.1347.016.

Arias, C., Sharma, N., Davies, P., Shafit-Zagardo, B., 1993. Okadaic acid induces early changes in microtubule-associated protein 2 and tau phosphorylation prior to neurodegeneration in cultured cortical neurons. J. Neurochem. 61 (2), 673–682. https://doi.org/10.1111/j.1471-4159.1993.tb02172.x.

Augustinack, J.C., Schneider, A., Mandelkow, E.M., Hyman, B.T., 2002. Specific tau phosphorylation sites correlate with severity of neuronal cytopathology in Alzheimer's disease. Acta Neuropathol. 103 (1), 26–35. https://doi.org/10.1007/s004010100423.

Ayciriex, S., Djelti, F., Alves, S., Regazzetti, A., Gaudin, M., Varin, J., Cartier, N., 2017. Neuronal cholesterol accumulation induced by Cyp46a1 down-regulation in mouse hippocampus disrupts brain lipid homeostasis. Front. Mol. Neurosci. 10, 211. https://doi.org/10.3389/fnmol.2017.00211.

Ballatore, C., Lee, V.M., Trojanowski, J.Q., 2007. Tau-mediated neurodegeneration in Alzheimer's disease and related disorders. Nat. Rev. Neurosci. 8 (9), 663–672. https://doi.org/10.1038/nrn2194.

Björkhem, I., Cedazo-Minguez, A., Leoni, V., Meaney, S., 2009. Oxysterols and neurodegenerative diseases. Mol. Asp. Med. 30 (3), 171–179. https://doi.org/10.1016/j.mam.2009.02.001.

Boussicault, L., Alves, S., Lamazière, A., Planques, A., Heck, N., Moumné, L., Betuing, S., 2016. CYP46A1, the rate-limiting enzyme for cholesterol degradation, is neuroprotective in Huntington's disease. Brain 139 (Pt 3), 953–970. https://doi.org/10.1093/brain/awv384.

Boussicault, L., Kacher, R., Lamazière, A., Vanhoutte, P., Caboche, J., Betuing, S., Potier, M.C., 2018. CYP46A1 protects against NMDA-mediated excitotoxicity in Huntington's disease: analysis of lipid raft content. Biochimie 153, 70–79. https://doi.org/10.1016/j.biochi.2018.07.019.

Brunden, K.R., Trojanowski, J.Q., Lee, V.M., 2008. Evidence that non-fibrillar tau causes pathology linked to neurodegeneration and behavioral impairments. J. Alzheimers Dis. 14 (4), 393–399. https://doi.org/10.3233/jad-2008-14406.

Brunello, C.A., Merezhko, M., Uronen, R.L., Huttunen, H.J., 2020. Mechanisms of secretion and spreading of pathological tau protein. Cell. Mol. Life Sci. 77 (9), 1721–1744. https://doi.org/10.1007/s00018-019-03349-1.

Burlot, M.A., Braudeau, J., Michaelsen-Preusse, K., Potier, B., Ayciriex, S., Varin, J., Cartier, N., 2015. Cholesterol 24-hydroxylase defect is implicated in memory impairments associated with Alzheimer-like tau pathology. Hum. Mol. Genet. 24 (21), 5965–5976. https://doi.org/10.1093/hmg/ddv268.

Caceres, A., Kosik, K.S., 1990. Inhibition of neurite polarity by tau antisense oligonucleotides in primary cerebellar neurons. Nature 343 (6257), 461–463. https://doi.org/10.1038/343461a0.

Chou, C.H., Yang, C.R., 2021. Neuroprotective studies of evodiamine in an okadaic acid-induced neurotoxicity. Int. J. Mol. Sci. 22 (10). https://doi.org/10.3390/ijms22105347.
Cleveland, D.W., Hwo, S.Y., Kirschner, M.W., 1977. Physical and chemical properties of purified tau factor and the role of tau in microtubule assembly. J. Mol. Biol. 116 (2), 227–247. https://doi.org/10.1016/0022-2836(77)90214-5.
Djelti, F., Braudeau, J., Hudry, E., Dhenain, M., Varin, J., Bièche, I., Cartier, N., 2015. CYP46A1 inhibition, brain cholesterol accumulation and neurodegeneration pave the way for Alzheimer's disease. Brain 138 (Pt 8), 2383–2398. https://doi.org/10.1093/brain/awv166.
Engel, T., Lucas, J.J., Gómez-Ramos, P., Moran, M.A., Avila, J., Hernández, F., 2006. Cooexpression of FTDP-17 tau and GSK-3beta in transgenic mice induce tau polymerization and neurodegeneration. Neurobiol. Aging 27 (9), 1258–1268. https://doi.org/10.1016/j.neurobiolaging.2005.06.010.
Fá, M., Puzzo, D., Piacentini, R., Staniszewski, A., Zhang, H., Baltrons, M.A., Arancio, O., 2016. Extracellular tau oligomers produce an immediate impairment of LTP and memory. Sci. Rep. 6, 19393. https://doi.org/10.1038/srep19393.
Ferrer, I., Blanco, R., Carmona, M., Ribera, R., Goutan, E., Puig, B., Ribalta, T., 2001. Phosphorylated map kinase (ERK1, ERK2) expression is associated with early tau deposition in neurones and glial cells, but not with increased nuclear DNA vulnerability and cell death, in Alzheimer disease, Pick's disease, progressive supranuclear palsy and corticobasal degeneration. Brain Pathol. 11 (2), 144–158. https://doi.org/10.1111/j.1750-3639.2001.tb00387.x.
Frost, B., Jacks, R.L., Diamond, M.I., 2009. Propagation of tau misfolding from the outside to the inside of a cell. J. Biol. Chem. 284 (19), 12845–12852. https://doi.org/10.1074/jbc.M808759200.
Gamba, P., Leonarduzzi, G., Tamagno, E., Guglielmotto, M., Testa, G., Sottero, B., Poli, G., 2011. Interaction between 24-hydroxycholesterol, oxidative stress, and amyloid-β in amplifying neuronal damage in Alzheimer's disease: three partners in crime. Aging Cell 10 (3), 403–417. https://doi.org/10.1111/j.1474-9726.2011.00681.x.
Gamba, P., Testa, G., Sottero, B., Gargiulo, S., Poli, G., Leonarduzzi, G., 2012. The link between altered cholesterol metabolism and Alzheimer's disease. Ann. N. Y. Acad. Sci. 1259, 54–64. https://doi.org/10.1111/j.1749-6632.2012.06513.x.
Gamba, P., Testa, G., Gargiulo, S., Staurenghi, E., Poli, G., Leonarduzzi, G., 2015. Oxidized cholesterol as the driving force behind the development of Alzheimer's disease. Front. Aging Neurosci. 7, 119. https://doi.org/10.3389/fnagi.2015.00119.
Gamba, P., Giannelli, S., Staurenghi, E., Testa, G., Sottero, B., Biasi, F., Leonarduzzi, G., 2021. The controversial role of 24-S-hydroxycholesterol in Alzheimer's disease. Antioxidants (Basel) 10 (5). https://doi.org/10.3390/antiox10050740.
Gordon-Weeks, P.R., Fournier, A.E., 2014. Neuronal cytoskeleton in synaptic plasticity and regeneration. J. Neurochem. 129 (2), 206–212. https://doi.org/10.1111/jnc.12502.
Grundke-Iqbal, I., Iqbal, K., Tung, Y.C., Quinlan, M., Wisniewski, H.M., Binder, L.I., 1986. Abnormal phosphorylation of the microtubule-associated protein tau (tau) in Alzheimer cytoskeletal pathology. Proc. Natl. Acad. Sci. USA 83 (13), 4913–4917. https://doi.org/10.1073/pnas.83.13.4913.
Guo, J.L., Lee, V.M., 2013. Neurofibrillary tangle-like tau pathology induced by synthetic tau fibrils in primary neurons over-expressing mutant tau. FEBS Lett. 587 (6), 717–723. https://doi.org/10.1016/j.febslet.2013.01.051.
Han, M., Wang, S., Yang, N., Wang, X., Zhao, W., Saed, H.S., Wang, J., 2020. Therapeutic implications of altered cholesterol homeostasis mediated by loss of CYP46A1 in human glioblastoma. EMBO Mol. Med. 12 (1), e10924. https://doi.org/10.15252/emmm.201910924.
Henkins, K.M., Sokolow, S., Miller, C.A., Vinters, H.V., Poon, W.W., Cornwell, L.B., Gylys, K.H., 2012. Extensive p-tau pathology and SDS-stable p-tau oligomers in Alzheimer's cortical synapses. Brain Pathol. 22 (6), 826–833. https://doi.org/10.1111/j.1750-3639.2012.00598.x.
Huang, J.M., Huang, F.I., Yang, C.R., 2019. Moscatilin ameliorates tau phosphorylation and cognitive deficits in Alzheimer's disease models. J. Nat. Prod. 82 (7), 1979–1988. https://doi.org/10.1021/acs.jnatprod.9b00375.
Hudry, E., Van Dam, D., Kulik, W., De Deyn, P.P., Stet, F.S., Ahouansou, O., Cartier, N., 2010. Adeno-associated virus gene therapy with cholesterol 24-hydroxylase reduces the amyloid pathology before or after the onset of amyloid plaques in mouse models of Alzheimer's disease. Mol. Ther. 18 (1), 44–53. https://doi.org/10.1038/mt.2009.175.
Johnson, G.V., Stoothoff, W.H., 2004. Tau phosphorylation in neuronal cell function and dysfunction. J. Cell Sci. 117 (Pt 24), 5721–5729. https://doi.org/10.1242/jcs.01558.
Khezri, M.R., Yousefi, K., Esmaeili, A., Ghasemnejad-Berenji, M., 2023. The role of ERK1/2 pathway in the pathophysiology of Alzheimer's disease: an overview and update on new developments. Cell. Mol. Neurobiol. 43 (1), 177–191. https://doi.org/10.1007/s10571-022-01191-x.
Kim, S.D., Yang, S.I., Kim, H.C., Shin, C.Y., Ko, K.H., 2007. Inhibition of GSK-3beta mediates expression of MMP-9 through ERK1/2 activation and translocation of NF-kappaB in rat primary astrocyte. Brain Res. 1186, 12–20. https://doi.org/10.1016/j.brainres.2007.10.018.
Kimura, T., Ishiguro, K., Hisanaga, S., 2014. Physiological and pathological phosphorylation of tau by Cdk5. Front. Mol. Neurosci. 7, 65. https://doi.org/10.3389/fnmol.2014.00065.
Knafo, S., Alonso-Nanclares, L., Gonzalez-Soriano, J., Merino-Serrais, P., Fernaud-Espinosa, I., Ferrer, I., DeFelipe, J., 2009. Widespread changes in dendritic spines in a model of Alzheimer's disease. Cereb. Cortex 19 (3), 586–592. https://doi.org/10.1093/cercor/bhn111.
Latorre-Leal, M., Rodriguez-Rodriguez, P., Franchini, L., Nikolidakis, O., Daniilidou, M., Delac, L., Maioli, S., 2024. CYP46A1-mediated cholesterol turnover induces sex-specific changes in cognition and counteracts memory loss in ovariectomized mice. Sci. Adv. 10 (4), eadj1354. https://doi.org/10.1126/sciadv.adj1354.
Leroy, K., Yilmaz, Z., Brion, J.P., 2007. Increased level of active GSK-3beta in Alzheimer's disease and accumulation in argyrophilic grains and in neurones at different stages of neurofibrillary degeneration. Neuropathol. Appl. Neurobiol. 33 (1), 43–55. https://doi.org/10.1111/j.1365-2990.2006.00795.x.
Linsenbardt, A.J., Taylor, A., Emnett, C.M., Doherty, J.J., Krishnan, K., Covey, D.F., Mennerick, S., 2014. Different oxysterols have opposing actions at N-methyl-D-aspartate receptors. Neuropharmacology 85, 232–242. https://doi.org/10.1016/j.neuropharm.2014.05.027.
Loera-Valencia, R., Goikolea, J., Parrado-Fernandez, C., Merino-Serrais, P., Maioli, S., 2019. Alterations in cholesterol metabolism as a risk factor for developing Alzheimer's disease: potential novel targets for treatment. J. Steroid Biochem. Mol. Biol. 190, 104–114. https://doi.org/10.1016/j.jsbmb.2019.03.003.
Lund, E.G., Xie, C., Kotti, T., Turley, S.D., Dietschy, J.M., Russell, D.W., 2003. Knockout of the cholesterol 24-hydroxylase gene in mice reveals a brain-specific mechanism of cholesterol turnover. J. Biol. Chem. 278 (25), 22980–22988. https://doi.org/10.1074/jbc.M303415200.
Ly, P.T., Wu, Y., Zou, H., Wang, R., Zhou, W., Kinoshita, A., Song, W., 2013. Inhibition of GSK3β-mediated BACE1 expression reduces Alzheimer-associated phenotypes. J. Clin. Invest. 123 (1), 224–235. https://doi.org/10.1172/JCI64516.
Maioli, S., Båvner, A., Ali, Z., Heverin, M., Ismail, M.A., Puerta, E., Björkhem, I., 2013. Is it possible to improve memory function by upregulation of the cholesterol 24S-hydroxylase (CYP46A1) in the brain? PLoS One 8 (7), e68534. https://doi.org/10.1371/journal.pone.0068534.
Mast, N., Lin, J.B., Anderson, K.W., Bjorkhem, I., Pikuleva, I.A., 2017a. Transcriptional and post-translational changes in the brain of mice deficient in cholesterol removal mediated by cytochrome P450 46A1 (CYP46A1). PLoS One 12 (10), e0187168. https://doi.org/10.1371/journal.pone.0187168.
Mast, N., Saadane, A., Valencia-Olvera, A., Constans, J., Maxfield, E., Arakawa, H., Pikuleva, I.A., 2017b. Cholesterol-metabolizing enzyme cytochrome P450 46A1 as a pharmacologic target for Alzheimer's disease. Neuropharmacology 123, 465–476. https://doi.org/10.1016/j.neuropharm.2017.06.026.
Mast, N., El-Darzi, N., Petrov, A.M., Li, Y., Pikuleva, I.A., 2020. CYP46A1-dependent and independent effects of efavirenz treatment. Brain Commun. 2 (2), fcaa180. https://doi.org/10.1093/braincomms/fcaa180.
Mast, N., Petrov, A.M., Prendergast, E., Bederman, I., Pikuleva, I.A., 2021. Brain acetyl-CoA production and phosphorylation of cytoskeletal proteins are targets of CYP46A1 activity modulation and altered sterol flux. Neurotherapeutics 18 (3), 2040–2060. https://doi.org/10.1007/s13311-021-01079-6.
Mast, N., Butts, M., Pikuleva, I.A., 2024. Unbiased insights into the multiplicity of the CYP46A1 brain effects in 5XFAD mice treated with low dose-efavirenz. J. Lipid Res. 65 (6), 100555. https://doi.org/10.1016/j.jlr.2024.100555.
Merino-Serrais, P., Benavides-Piccione, R., Blazquez-Llorca, L., Kastanauskaite, A., Rábano, A., Avila, J., DeFelipe, J., 2013. The influence of phospho-τ on dendritic spines of cortical pyramidal neurons in patients with Alzheimer's disease. Brain 136 (Pt 6), 1913–1928. https://doi.org/10.1093/brain/awt088.
Merino-Serrais, P., Loera-Valencia, R., Rodriguez-Rodriguez, P., Parrado-Fernandez, C., Ismail, M.A., Maioli, S., Cedazo-Minguez, A., 2019. 27-hydroxycholesterol induces aberrant morphology and synaptic dysfunction in hippocampal neurons. Cereb. Cortex 29 (1), 429–446. https://doi.org/10.1093/cercor/bhy274.
Mitroi, D.N., Pereyra-Gómez, G., Soto-Huelin, B., Senovilla, F., Kobayashi, T., Esteban, J. A., Ledesma, M.D., 2019. NPC1 enables cholesterol mobilization during long-term potentiation that can be restored in Niemann-Pick disease type C by CYP46A1 activation. EMBO Rep. 20 (11), e48143. https://doi.org/10.15252/embr.201948143.
Muñoz-Lasso, D.C., Romá-Mateo, C., Pallardó, F.V., Gonzalez-Cabo, P., 2020. Much more than a scaffold: cytoskeletal proteins in neurological disorders. Cells 9 (2). https://doi.org/10.3390/cells9020358.
Niewiadomska, G., Niewiadomski, W., Steczkowska, M., Gasiorowska, A., 2021. Tau oligomers neurotoxicity. Life (Basel) 11 (1). https://doi.org/10.3390/life11010028.
Nóbrega, C., Mendonça, L., Marcelo, A., Lamazière, A., Tomé, S., Despres, G., Alves, S., 2019. Restoring brain cholesterol turnover improves autophagy and has therapeutic potential in mouse models of spinocerebellar ataxia. Acta Neuropathol. 138 (5), 837–858. https://doi.org/10.1007/s00401-019-02019-7.
Okabe, A., Urano, Y., Itoh, S., Suda, N., Kotani, R., Nishimura, Y., Noguchi, N., 2013. Adaptive responses induced by 24S-hydroxycholesterol through liver X receptor pathway reduce 7-ketocholesterol-caused neuronal cell death. Redox Biol. 2, 28–35. https://doi.org/10.1016/j.redox.2013.11.007.
Patrick, G.N., Zukerberg, L., Nikolic, M., de la Monte, S., Dikkes, P., Tsai, L.H., 1999. Conversion of p35 to p25 deregulates Cdk5 activity and promotes neurodegeneration. Nature 402 (6762), 615–622. https://doi.org/10.1038/45159.
Paul, S.M., Doherty, J.J., Robichaud, A.J., Belfort, G.M., Chow, B.Y., Hammond, R.S., Zorumski, C.F., 2013. The major brain cholesterol metabolite 24(S)-hydroxycholesterol is a potent allosteric modulator of N-methyl-D-aspartate receptors. J. Neurosci. 33 (44), 17290–17300. https://doi.org/10.1523/JNEUROSCI.2619-13.2013.
Pei, J.J., Braak, H., An, W.L., Winblad, B., Cowburn, R.F., Iqbal, K., Grundke-Iqbal, I., 2002. Up-regulation of mitogen-activated protein kinases ERK1/2 and MEK1/2 is associated with the progression of neurofibrillary degeneration in Alzheimer's disease. Brain Res. Mol. Brain Res. 109 (1–2), 45–55. https://doi.org/10.1016/s0169-328x(02)00488-6.
Petrov, A.M., Mast, N., Li, Y., Pikuleva, I.A., 2019. The key genes, phosphoproteins, processes, and pathways affected by efavirenz-activated CYP46A1 in the amyloid-decreasing paradigm of efavirenz treatment. FASEB J. 33 (8), 8782–8798. https://doi.org/10.1096/fj.201900092R.

Petrov, A.M., Mast, N., Li, Y., Denker, J., Pikuleva, I.A., 2020. Brain sterol flux mediated by cytochrome P450 46A1 affects membrane properties and membrane-dependent processes. Brain Commun. 2 (1). https://doi.org/10.1093/braincomms/fcaa043.

Popiolek, M., Izumi, Y., Hopper, A.T., Dai, J., Miller, S., Shu, H.J., Mennerick, S., 2020. Effects of CYP46A1 inhibition on long-term-depression in hippocampal slices. Front. Mol. Neurosci. 13, 568641. https://doi.org/10.3389/fnmol.2020.568641.

Prasanthi, J.R., Huls, A., Thomasson, S., Thompson, A., Schommer, E., Ghribi, O., 2009. Differential effects of 24-hydroxycholesterol and 27-hydroxycholesterol on beta-amyloid precursor protein levels and processing in human neuroblastoma SH-SY5Y cells. Mol. Neurodegener. 4, 1. https://doi.org/10.1186/1750-1326-4-1.

Seo, J., Kritskiy, O., Watson, L.A., Barker, S.J., Dey, D., Raja, W.K., Tsai, L.H., 2017. Inhibition of p25/Cdk5 attenuates tauopathy in mouse and iPSC models of frontotemporal dementia. J. Neurosci. 37 (41), 9917–9924. https://doi.org/10.1523/JNEUROSCI.0621-17.2017.

Shafaati, M., Olin, M., Båvner, A., Pettersson, H., Rozell, B., Meaney, S., Björkhem, I., 2011. Enhanced production of 24S-hydroxycholesterol is not sufficient to drive liver X receptor target genes in vivo. J. Intern. Med. 270 (4), 377–387. https://doi.org/10.1111/j.1365-2796.2011.02389.x.

Sontag, J.M., Sontag, E., 2014. Protein phosphatase 2A dysfunction in Alzheimer's disease. Front. Mol. Neurosci. 7, 16. https://doi.org/10.3389/fnmol.2014.00016.

Spillantini, M.G., Goedert, M., 2013. Tau pathology and neurodegeneration. Lancet Neurol. 12 (6), 609–622. https://doi.org/10.1016/S1474-4422(13)70090-5.

Staurenghi, E., Cerrato, V., Gamba, P., Testa, G., Giannelli, S., Leoni, V., Leonarduzzi, G., 2021. Oxysterols present in Alzheimer's disease brain induce synaptotoxicity by activating astrocytes: a major role for lipocalin-2. Redox Biol. 39, 101837. https://doi.org/10.1016/j.redox.2020.101837.

Tai, H.C., Wang, B.Y., Serrano-Pozo, A., Frosch, M.P., Spires-Jones, T.L., Hyman, B.T., 2014. Frequent and symmetric deposition of misfolded tau oligomers within presynaptic and postsynaptic terminals in Alzheimer's disease. Acta Neuropathol. Commun. 2, 146. https://doi.org/10.1186/s40478-014-0146-2.

Takahashi, M., Nakabayashi, T., Mita, N., Jin, X., Aikawa, Y., Sasamoto, K., Ohshima, T., 2022. Involvement of Cdk5 activating subunit p35 in synaptic plasticity in excitatory and inhibitory neurons. Mol. Brain 15 (1), 37. https://doi.org/10.1186/s13041-022-00922-x.

Tanaka, T., Ohashi, S., Takashima, A., Kobayashi, S., 2022. Dendritic distribution of CDK5 mRNA and p35 mRNA, and a glutamate-responsive increase of CDK5/p25 complex contribute to tau hyperphosphorylation. Biochim. Biophys. Acta Gen. Subj. 1866 (7), 130135. https://doi.org/10.1016/j.bbagen.2022.130135.

Testa, G., Gamba, P., Badilli, U., Gargiulo, S., Maina, M., Guina, T., Leonarduzzi, G., 2014. Loading into nanoparticles improves quercetin's efficacy in preventing neuroinflammation induced by oxysterols. PLoS One 9 (5), e96795. https://doi.org/10.1371/journal.pone.0096795.

Testa, G., Staurenghi, E., Zerbinati, C., Gargiulo, S., Iuliano, L., Giaccone, G., Gamba, P., 2016. Changes in brain oxysterols at different stages of Alzheimer's disease: their involvement in neuroinflammation. Redox Biol. 10, 24–33. https://doi.org/10.1016/j.redox.2016.09.001.

Testa, G., Staurenghi, E., Giannelli, S., Gargiulo, S., Guglielmotto, M., Tabaton, M., Leonarduzzi, G., 2018. A silver lining for 24-hydroxycholesterol in Alzheimer's disease: the involvement of the neuroprotective enzyme sirtuin 1. Redox Biol. 17, 423–431. https://doi.org/10.1016/j.redox.2018.05.009.

Testa, G., Giannelli, S., Sottero, B., Staurenghi, E., Giaccone, G., Caroppo, P., Leonarduzzi, G., 2023. 24-hydroxycholesterol induces tau proteasome-dependent degradation via the SIRT1/PGC1α/Nrf2 pathway: a potential mechanism to counteract Alzheimer's disease. Antioxidants (Basel) 12 (3). https://doi.org/10.3390/antiox12030631.

Tseng, H.C., Zhou, Y., Shen, Y., Tsai, L.H., 2002. A survey of Cdk5 activator p35 and p25 levels in Alzheimer's disease brains. FEBS Lett. 523 (1–3), 58–62. https://doi.org/10.1016/s0014-5793(02)02934-4.

Tuck, B.J., Miller, L.V.C., Katsinelos, T., Smith, A.E., Wilson, E.L., Keeling, S., McEwan, W.A., 2022. Cholesterol determines the cytosolic entry and seeded aggregation of tau. Cell Rep. 39 (5), 110776. https://doi.org/10.1016/j.celrep.2022.110776.

Urano, Y., Ochiai, S., Noguchi, N., 2013. Suppression of amyloid-β production by 24S-hydroxycholesterol via inhibition of intracellular amyloid precursor protein trafficking. FASEB J. 27 (10), 4305–4315. https://doi.org/10.1096/fj.13-231456.

van der Kant, R., Langness, V.F., Herrera, C.M., Williams, D.A., Fong, L.K., Leestemaker, Y., Goldstein, L.S.B., 2019. Cholesterol metabolism is a druggable axis that independently regulates tau and amyloid-β in iPSC-derived Alzheimer's disease neurons. Cell Stem Cell 24 (3), 363–375 e369. https://doi.org/10.1016/j.stem.2018.12.013.

van der Kant, R., Goldstein, L.S.B., Ossenkoppele, R., 2020. Amyloid-β-independent regulators of tau pathology in Alzheimer disease. Nat. Rev. Neurosci. 21 (1), 21–35. https://doi.org/10.1038/s41583-019-0240-3.

Varma, V.R., Büşra Lüleci, H., Oommen, A.M., Varma, S., Blackshear, C.T., Griswold, M. E., Thambisetty, M., 2021. Abnormal brain cholesterol homeostasis in Alzheimer's disease-a targeted metabolomic and transcriptomic study. NPJ Aging Mech. Dis. 7 (1), 11. https://doi.org/10.1038/s41514-021-00064-9.

Vauzour, D., Corsini, S., Müller, M., Spencer, J.P.E., 2018. Inhibition of PP2A by hesperetin may contribute to Akt and ERK1/2 activation status in cortical neurons. Arch. Biochem. Biophys. 650, 14–21. https://doi.org/10.1016/j.abb.2018.04.020.

Wei, X., Nishi, T., Kondou, S., Kimura, H., Mody, I., 2019. Preferential enhancement of GluN2B-containing native NMDA receptors by the endogenous modulator 24S-hydroxycholesterol in hippocampal neurons. Neuropharmacology 148, 11–20. https://doi.org/10.1016/j.neuropharm.2018.12.028.

Wu, J.W., Herman, M., Liu, L., Simoes, S., Acker, C.M., Figueroa, H., Duff, K.E., 2013. Small misfolded tau species are internalized via bulk endocytosis and anterogradely and retrogradely transported in neurons. J. Biol. Chem. 288 (3), 1856–1870. https://doi.org/10.1074/jbc.M112.394528.

Yamanaka, K., Saito, Y., Yamamori, T., Urano, Y., Noguchi, N., 2011. 24(S)-hydroxycholesterol induces neuronal cell death through necroptosis, a form of programmed necrosis. J. Biol. Chem. 286 (28), 24666–24673. https://doi.org/10.1074/jbc.M111.236273.

Zhang, Z., Simpkins, J.W., 2010a. An okadaic acid-induced model of tauopathy and cognitive deficiency. Brain Res. 1359, 233–246. https://doi.org/10.1016/j.brainres.2010.08.077.

Zhang, Z., Simpkins, J.W., 2010b. Okadaic acid induces tau phosphorylation in SH-SY5Y cells in an estrogen-preventable manner. Brain Res. 1345, 176–181. https://doi.org/10.1016/j.brainres.2010.04.074.

Zhang, W., Yang, J., Liu, Y., Chen, X., Yu, T., Jia, J., Liu, C., 2009. PR55 alpha, a regulatory subunit of PP2A, specifically regulates PP2A-mediated beta-catenin dephosphorylation. J. Biol. Chem. 284 (34), 22649–22656. https://doi.org/10.1074/jbc.M109.013698.

Zhou, J., Wang, H., Feng, Y., Chen, J., 2010. Increased expression of cdk5/p25 in N2a cells leads to hyperphosphorylation and impaired axonal transport of neurofilament proteins. Life Sci. 86 (13–14), 532–537. https://doi.org/10.1016/j.lfs.2010.02.009.